REPORT DOCUMENTATION PAGE

Form Approved
OMB NO. 0704-0188

1. AGENCY USE ONLY (Leave Blank)	2. REPORT DATE	3. REPORT TYPE AND DATES COVERED
	03/31/06	Final Report 01 Aug 02 - 31 Dec 05

4. TITLE AND SUBTITLE

TIME RESOLVED MEASUREMENTS AND REACTIVE PATHWAYS OF HYPERGOLIC BIPROPELLANT COMBUSTION

5. FUNDING NUMBERS

DAAD19-02-1-0356

6. AUTHOR(S)

Dr. James E. Smith Jr.

7. PERFORMING ORGANIZATION NAME(S) AND ADDRESS(ES)

University of Alabama in Huntsville
301 Sprakman Drive Huntsville, AL 35899

8. PERFORMING ORGANIZATION REPORT NUMBER

9. SPONSORING / MONITORING AGENCY NAME(S) AND ADDRESS(ES)

U. S. Army Research Office
P.O. Box 12211
Research Triangle Park, NC 27709-2211

10. SPONSORING / MONITORING AGENCY REPORT NUMBER

41691.10-EG

11. SUPPLEMENTARY NOTES

The views, opinions and/or findings contained in this report are those of the author(s) and should not be construed as an official Department of the Army position, policy or decision, unless so designated by other documentation.

12 a. DISTRIBUTION / AVAILABILITY STATEMENT

Approved for public release; distribution unlimited.

12 b. DISTRIBUTION CODE

13. ABSTRACT (Maximum 200 words)

This research has improved the fundamental understanding of the physical mechanisms leading to the ignition and combustion of hypergolic propellants from high-speed visualization and combustion diagnostics. The laser diagnostic system for the measurement of hypergolic droplet mixing and combustion was further developed by controlling many relevant factors. These include: droplet size, impact, and mixing; fuel/oxidizer lead; fuel/oxidizer ratio; controlled atmosphere, chemical safety, and event timing and resolution. As a result, a previous qualitative method was converted to a highly sensitive quantitative method capable of capturing subtleties in hypergolic bipropellant combustion including: effects of atmospheric air and moisture; carbon/nitrogen ratio within mixed hydrazines; oxygenation of Hydrazine/UDMH mixtures; the effect of additives on MMH, particular the MMH/Methanol system; temperature effects on CDT; kinetic modeling of the chemical delay time, liquid reaction time, and proposed reaction mechanism for Anhydrous Hydrazine/RFNA; preliminary investigations into the liquid reaction temperature prior to combustion; and CDT data and kinetic parameters determined where possible for “green fuels” replacements under development by AMRDEC.

Methods were developed to correlate the chemical delay time and liquid reaction times, and ultimately produced bulk kinetic data. These methods have been well received resulting in significant technology transfer.

14. SUBJECT TERMS

Chemical Delay Time
Hypergolic Bipropellants

15. NUMBER OF PAGES

39

16. PRICE CODE

17. SECURITY CLASSIFICATION OR REPORT	18. SECURITY CLASSIFICATION ON THIS PAGE	19. SECURITY CLASSIFICATION OF ABSTRACT	20. LIMITATION OF ABSTRACT
UNCLASSIFIED	**UNCLASSIFIED**	**UNCLASSIFIED**	**UL**

NSN 7540-01-280-5500

Standard Form 298 (Rev.2-89)
Prescribed by ANSI Std. 239-18
298-102

TABLE OF CONTENTS

LIST OF FIGURES

LIST OF TABLES

1.0 STATEMENT AND OBJECTIVES OF PROBLEM STUDIED

The combustor and spectroscopic analysis system for the measurement of hypergolic droplet mixing and combustion was further developed. Using this device we identified both the chemical delay time and liquid reaction time and their significance to chemical performance in hypergolic combustion. However, only limited data of classical hypergolic systems existed and no definitive data on the spectroscopic signature of the free radicals generated just prior to combustion is available. The signal decrease on entry into the CDT region was to be used to trigger the Nd:Yag laser and Near-IR spectrometer with an optical multi-channel analyzer in an attempt to collect the Raman signature of the free radicals just prior to, during and after combustion. Thus, the objectives were to collect additional CDT data on classical hypergolic combustibles and attempt to determine their free radical chemistry using both Visible and Near-IR Raman Spectroscopy, (Fadini and Schnepel 1989). Both units can be configured to study emission spectroscopy once the flame has ignited, however our focus was to examine the reactants evolving from the liquid phase just prior to the combustion process. Examining regions within the ignition delay time is only possible using the laser diagnostic method as detailed later. Understanding how these materials combust, has increased our overall knowledge of the phenomena and permitted the advancement of both traditional and newly formulated amine/azide hypergolic fuels that are less hazardous to humans and the environment while possibly leading to propulsion system replacement candidates and direct improvements of hypergolic bipropellants systems. The original objectives were as follows:

1. Collect additional Chemical Delay Time data on traditional hypergolic bipropellants and determine free radical chemistry using Emission, Visible and Near-IR Raman Spectroscopy in the pre-ignition and combustion phases of traditional hypergolic bipropellants.
2. Correlate the combustion chemistry with the Chemical Delay Time (CDT) and determine if the slope of the ignition signal is related to flame propagation speed using high speed imaging techniques.
3. Examine fuel mixtures to determine if there are synergistic relationships between fuel mixture decomposition and free radical generation as seen by spectroscopic means and the chemical delay time.
4. Improved the fundamental understanding of the physical mechanisms leading to the ignition and combustion of hypergolic propellants from high-speed visualization and combustion diagnostics.
5. Extend our chemical understanding to newly formulated amine/azide fuels to determine their ignition and chemical delay times in comparison to currently deployed hypergolic bipropellants.
6. Evaluate amine/azide fuel mixture to determine if they exhibit synergistic hypergolic ignition that could also lower their overall ignition delay time as seen in hydrazine-UDMH mixtures.

A detailed chemical knowledge of hypergolic combustion, combined with advanced timing techniques based on the chemical delay time, should permit the analysis of chemical pathways and free radicals generated in the pre-ignition phase. Such advances will enable tailoring of mixed organic phases with either less toxic or non-toxic species while producing acceptable ignition time delays for engine development. The ultimate goal will be to develop “green chemistry” for use in hypergolic rocket engines important to the mission of the U.S. Army.

1.1 Overview of Accomplishments and Introduction to the Technical Report

The majority of the above six objectives were met or exceeded with the exception of the spectroscopic methods, where the Optical Multi-Channel Analyzers required a minimum exposure time, too long to capture the specific regions outlined in objective 1. The OMAs typically saturated due to the fluorescence and bulk emission that resulted from the combustion. The events in objective 1 could not be separated into distinct regions once the ultimate resolution of the modified Laser Diagnostic Technique was developed. Methods were developed to correlate the chemical delay time and liquid reaction times, and ultimately produced bulk kinetic data as outlined in the following technical report. These methods have been well received resulting in significant technology transfer.

1.2 Previous Ignition Delay Time Literature Review

Diagnostic techniques that measure ignition delay times of hypergolic bipropellants are normally classified into a few distinct types. Drop tests are techniques that drop one reactant from a set height into a stationary quantity of the second reactant. Mixing tests are techniques that use a method to enhance mixing of the reactant combinations. Impinging jet techniques are tests that use separate fuel and oxidizer injectors to enhance the mixing rate and

simulate engine conditions. Also, a few small scale rocket engines have been equipped to measure ignition delay times.

A typical example of a drop test technique was performed by Broatch (1950) and is shown in Figure 1 (Broatch 1950). In this setup, a light beam was focused on a photocell a set distance above the organic fuel located in a crucible. The oxidizer, in a stream of droplets of varying size, broke the light beam as it fell into the fuel. These droplets contacted the fuel at varying times, with the initial droplet being the reference for the ignition delay measurement. A photocell ended the measurement when it sensed the appearance of a flame. The time between these two events defined the ignition delay for the hypergolic bipropellant. Since the droplets entered the oxidizer at varying times, the ignition delay was not well defined. In addition, this meant that the oxidizer to fuel ratio could not be defined by Broatch's technique.

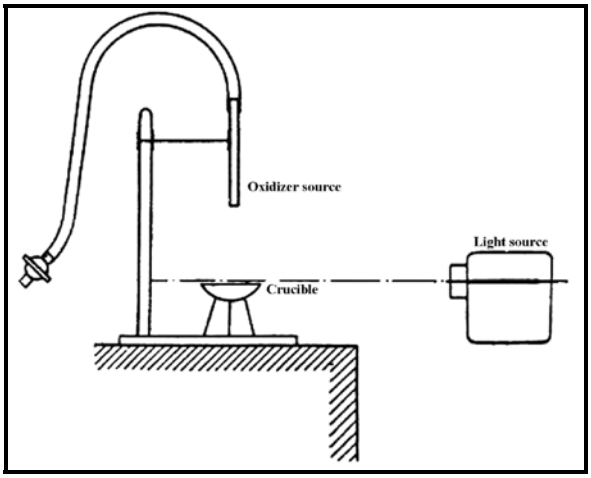

Figure 1: Broatch's, 1950 Drop Test Apparatus

A technique used by Gunn (1952) was defined as a mixing test by Paushkin (1962) in his review of jet fuels. The only significant difference from Broatch's technique described above was that the quantity of fuel and oxidizer used by Gunn was several times larger. Several milliliters of one reactant were decanted into a similar quantity of the other reactant. The start of timing was due to the completion of an electrical circuit. This was achieved by contact between the fuel and oxidizer. The end of timing was obtained by the response of a photocell to the appearance of flame, similar to Broatch's technique. The photocell used by Gunn to detect the flame, and the one used in Broatch's technique above, did not indicate the strength of the reaction. These photocells only indicated the end of an ignition delay measurement. The technique presented here, does provide insight into the combustion rate.

The device constructed by Pino (1955) caused the pressurized injection of oxidizer through 4 ports directed into a stationary quantity of fuel. The pressurized injection enhanced mixing of the reactants. The combined quantity of fuel and oxidizer used was approximately 4 milliliters for one test. Again, the start of timing was due to the completion of an electrical circuit between the reactants. The end of timing was sensed electrically due to the ionizing effect of the flame. The results of Pino's testing show no indication of the oxidizer to fuel ratio. The measuring technique only captures the ignition delay time. No additional phenomena were noted.

Ladanyi and Miller (1956) placed a small glass ampoule containing approximately one milliliter of fuel under the surface of several milliliters of oxidizer. The glass ampoule was crushed by a steel rod to enhance mixing. The initial time began at the moment of ampoule fractured. This was detected by the completion of an electrical circuit between a weight used to supply the downward force to the steel rod and the steel rod itself. The final measurement was made by a photocell sensing the appearance of a flame. The authors stated in the paper that mixing rate varied from test to test due to differences in the ampoules. Oxidizer to fuel ratio was not defined and varied during testing. Ignition delay times are a function of both mixing rate and oxidizer to fuel ratio.

Kilpatrick and Baker (1955) used a device that forced both fuel and oxidizer together using high-pressure gas hydraulics. The reactants were initially located in separate chambers below pistons which forced the propellants together immediately prior to injection into the combustion chamber. The initiation of the timing measurement was through monitoring of piston movement above the fuel and oxidizer. The end of an ignition delay measurement corresponded to an increase of pressure in the test chamber, which had a volume of 339 cm^3. This was corrected for the response time of a pressure gage located 0.5 meters from the chamber. The test results using the laser diagnostic approach show that significant vapor volume is created locally by the bipropellants just prior to ignition. Their test

did not indicate any attempt to obtain pressure values that consider this phenomenon for the fuels tested. In addition, this pressure rise could originate anywhere in the test chamber affecting pressure gage response time. These two factors limit the accuracy of the measurements made using this equipment. This technique did control oxidizer to fuel ratio, but provided no additional information other than the ignition delay time.

Saad and Goldwasser (1969) used impinging fuel and oxidizer jets in their technique. They initiated the ignition delay measurement at the moment the valves for fuel and oxidizer were released. Photocell detection of the flame was again used to end the measurement. The resolution of their oscilloscope was 100 milliseconds/division. As ignition delay values are generally less than 100 milliseconds, the resolution of their technique does not provide the accuracy needed for reactions of this speed. They initiated the ignition delay measurement from the moment the valves for fuel and oxidizer were released. The technique did not measure from the moment of impingement. These measurements are not ignition delays, as defined in the literature.

In addition to the drop test technique reported earlier, Broatch also used the technique of impinging jets (Broatch 1950). He used high-speed photography to capture pictures of the combined jets and flame. The ignition delay was calculated from the length of the combined jets to the fully developed flame front. No consideration was observed in the paper for the possibility of flame propagation upstream or downstream. No attempt was made to record the moment of ignition. Again, these measurements do not represent ignition delays. The benefits of the photography technique were to capture the strength of the flame as Broatch varied oxidizer to fuel ratio and temperature, and the ability to photograph phenomena such as pre-ignition boiling of the liquid phase.

Spengler and Bauer (1966) used impinging jets to test the influence of pressure and varying chemical composition on ignition delay measurements. This technique consisted of starting the timing by contacting the fuel and oxidizer, which completed an electrical circuit. The timing measurement was ended by sensing the flame with a photocell located between the two injectors. This technique for impinging jets seemed to be the only true measure of ignition delay among the three discussed. However, once again, the technique for measuring the ignition delay provided no additional information.

In review, several types of ignition delay techniques have been examined. They vary in complexity, cost and ability to measure ignition delay. The design of an ignition delay apparatus is heavily dependent upon the transport and mixing portion of the ignition delay time measurement and not on the chemical delay time, which is directly tied to the chemical reaction rate.

If the intent of the ignition delay technique is to screen hypergolic bipropellants, then the tests described above provide qualitative information that is device specific. However if one seeks quantitative data that can directly compare chemical performance of hypergolic bipropellant reactants detailed control of the parameters and times scales are needed.

In the sections that follow are descriptions of either fluid parameters or measurements accuracy that must be considered to develop a laser diagnostic technique capable of accurately and reproducibility measuring the chemical delay time inherently embedded within the ignition delay typically measure using qualitative techniques. As will be shown, the chemical delay time is independent of the mixing technique but not the fuel to oxidizer ratio.

1.3 Issues Relevant to the Development of the Laser Diagnostic Technique

In the development of the laser diagnostic technique, many relevant factors must be controlled to well-defined levels. These include, droplet size, impact, and mixing; fuel versus oxidizer lead; fuel to oxidizer ratio; controlled atmosphere, chemical safety, and finally event timing and resolution. As a result of this research, a previous qualitative method was converted to a highly sensitive quantitative method capable of capturing subtleties in hypergolic bipropellant combustion and evaluating bulk kinetics in both the gas and liquid phases. In the following sections the relevant issues are briefly discussed.

1.3.1 Droplet Size, Impact and Mixing

The most important variable to manage in drop-on-drop experiments, that are central to the laser diagnostic technique, is droplet size. The importance of droplet size was reviewed by Schmidt, 2001. From Figure 2, Schmidt suggests that droplet size selection should be kept in the linear region. However, very small droplets are difficult to reproduce increasing the experimental error, but smaller droplets approach the bipropellant model. Based on average droplet volumes the average droplet diameter for drop-on-drop experiments conducted with the laser diagnostic system was 1.2 mm (0.12 cm). This average droplet size is plotted in Figure 2, relative to the results reported by Schmidt and is very close to that required for the bipropellant model. Small droplets are said to remain in the evaporative or kinetic controlled mode, whereas large droplets are subject to diffusion-controlled combustion. Thus for controlled drop-on-drop experiments smaller drops that remain in the evaporative or kinetic controlled mode are preferred.

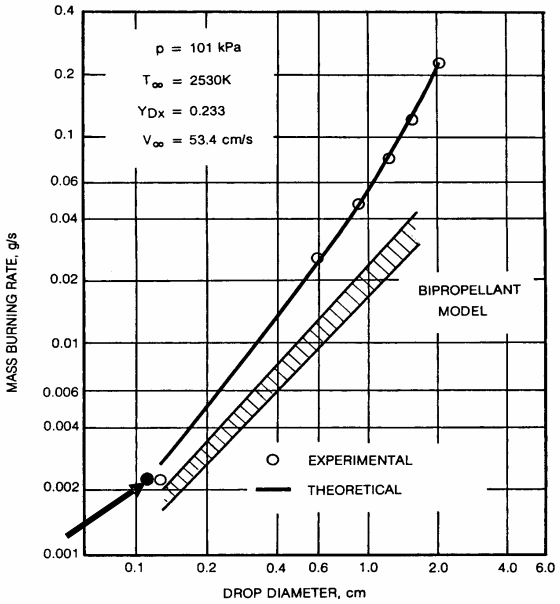

Figure 2: Bipropellant Model for Combustion (Schmidt, 2001)

1.3.2 Minimize Splashing and Bouncing

Purvis and Smith performed experiments investigating the splashing associated with a droplet falling into a layer of water (Purvis and Smith, 2004). It was discovered that large droplets produce more splash than smaller droplets. When the droplet was dropped into the layer of water, the crown formed by the droplet entering the layer of water consists mostly of water from the layer fluid being splashed away rather than the splash consisting of droplet fluid. However, as the ratio of droplet diameter to the depth of the layer increased, the splash consisted more of the droplet fluid. The amount of fluid splashed by such an impact was examined and found to increase with droplet size and to be significantly influenced by surface roughness. Surface roughness does have a significant effect on the amount of fluid ejected especially when the height of the roughness is comparable with the depth of the layer. This corresponds with the idea that the pool that the droplet falls into should be placed in a relatively smooth surface with the depth of the pool maximized. For the Laser Diagnostic System, smooth conical or bowl shaped combustor plates were employed. The initial droplet shape was shown to be less crucial, with slight deformations having little difference on splashing.

Pan and Law, 2004, performed experimental and simulation research on the dynamics of head-on droplet collision. The collision of two impinging droplets were studied and it was discovered that the instant at which two interfaces suddenly "wet" each other was the moment of coalescence; prior to this event, it is merely droplet collision. It was shown that the phenomena of coalescence and bouncing is differentiated by the relationship of the Weber number and the impact number, which relate to the droplet radius, relative velocity, distance between the drop centers in the direction normal to the relative velocity, liquid density and liquid surface tension (Qian and Law, 1997). The Weber number represents the ratio between the initial kinetic energy and surface energy of the droplet, while the impact number represents the range of collisions from head-on to grazing blows.

It was shown that five distinct regimes of the collision outcome between two identical droplets were identified based on the Weber number and the impact number. The five regimes were categorized according to: (I) permanent coalescence after minor droplet deformation, (II) bouncing, (III) permanent coalescence after substantial droplet deformation, (IV) coalescence followed by separation for near head-on collisions and (V) coalescence followed by separation for sufficiently off-center collisions. For reproducible drop-on-drop combustion experiments it is important to remain within the regime of permanent coalescence after minor droplet deformation (regime I) because this regime exhibits smaller kinetic energy and larger surface energy, as well as suffering less distortion and dissipative loss. The drop-on-drop experiments discussed within this report are within regime I, based on small droplet diameters, small droplet velocity due to short falling distances, and the fact that the droplet collisions are head-on as a result of using a multi-axis positioner such that the falling droplet is precisely located over the pool center.

1.3.3 Vortex Mixing Enhances Reactive Dynamics

If the droplets impact at the correct energy they must mix to chemically react. This mixing typically forms a vortex ring as described by Dooley et al., 1997. They performed an excellent series of experiments on drop-on-drop fluid mixing. They collected high speed photographs of laser excited fluoresce of water droplets, one with and one without a fluorescent dye. They detected and subsequently modeled vortex rings generated during the coalescence of a water droplet at a free water surface. Figure 3 shows their results which are included here to help the reader understand results discussed above and later in this report (Dooley et al. 1997). The vortices, shown in this Figure 3 (e-h), control the mixing of these homogeneous fluids. For bipropellant droplet tests using a fuel lead, an oxidizer droplet falls into a pool of fuel (points A-C in Figure 4 and a-h in Figure 3 shown below).

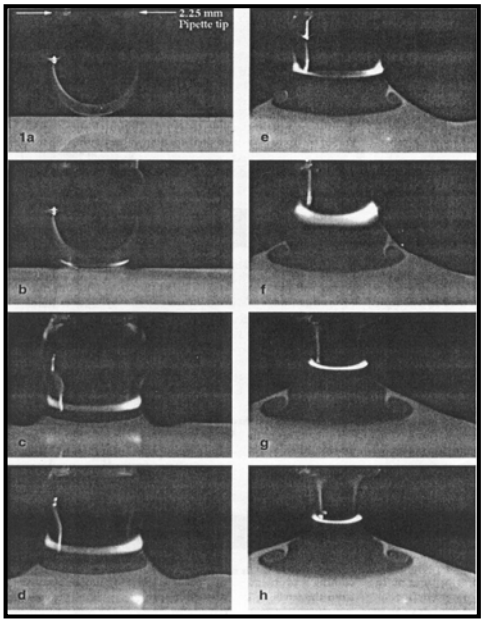

Figure 3: Vortex Ring Generation Due to the Coalescence of a Water Drop at a Free Surface (Dooley et al. 1997)

This vortex ring mixes the acid and base in a violent reaction front that can locally alter the oxidizer to fuel ratio producing a host of transport phenomena if the droplet dynamics are not considered, including: popping, film boiling, micro-explosions, liquid ejection, and splashing. These phenomena were researched by Farmer (1997) and Mays (1998). As the drop-on-drop technique advanced with greater impact and droplet size control more reproducible results were obtained. Figure 4 show a controlled drop-on-drop experiment that demonstrates a symmetric droplet falling into a pool of reactive liquid (A-B), reactive mixing (points B-C), followed by gas release and combustion (points C-D).

Due to vortex ring formation, at high oxidizer to fuel ratios, the size of the pool will self limit the combustion due to mass transfer limitations along the free surface of the reactive media. The excess fuel or oxidizer outside the ring will remain within the combustor. This was confirmed experimentally, when an additional drop of fuel was added to the combustor after an initial experiment at high oxidizer/fuel ratios without adding additional oxidizer. A flame consistently formed when the oxidizer/fuel ratio exceeded approximately 3. In essence, the vortex ring creates a micro reactor within the oxidizer pool. The vortex ring constrains the fuel droplet resulting in burning in the central region of the pool. What is not shown in Figure 3 is that the combustion front is not only controlled by vortex ring mixing, but also by the total external contact area of the drop, depth of the oxidizer pool, and density differences between the fuel and oxidizer that alters the impact inertia of the drop on the liquid pool. The strength of the droplet is controlled by the surface tension and contact angle between the two reactants.

The combustor geometry used to measure the data in our early research may have contributed to the problem of vortex ring confinement Framer, 1997 and Mays 1998. Measurements of the droplet size and the resulting vortex ring size permitted the design of several drop test combustors of smaller diameter and greater depth to better confine the lead component and minimize droplet dynamic effects, thus increasing the mixing rate.

An increase in the depth of the pool improves impact mixing and prevents burn-out in the core. A benefit of these revised designs is the reduction of the free surface of the lead component that reduces the degree of

evaporative losses from the pool. The careful control of droplet size, impact energy and pool size provided control of the fuel to oxidizer ratio in drop-on-drop experiments.

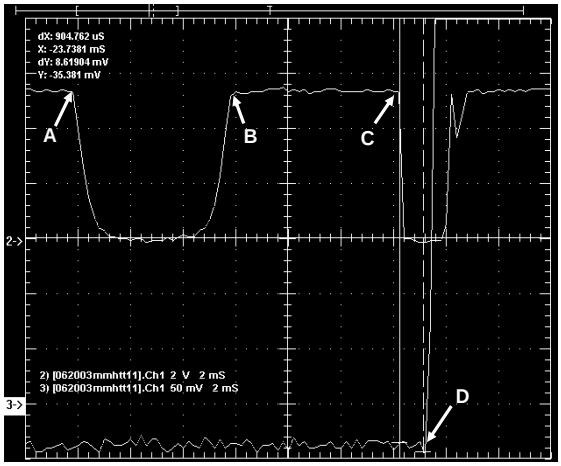

Figure 4: MMH/RFNA Data at a Fuel/Oxidizer Ratio of 1/3

1.3.4 Combustor Purge

Literature data for anhydrous hydrazine (AH) and MMH combustion in air showed that the reaction rate was directly proportional to oxygen mass fraction as shown in Figure 5 (Schmidt 2001). Standard deviation improved once an air purge was incorporated. Products and reactants heavier than air collect in the chamber reducing oxygen mass fraction. Figure 5 also shows that MMH reacts slower with air than Hydrazine. Thus, the principle fuels MMH and AH, in addition to reacting with the oxidizer, can also react with air.

The results section further expands on the need for an inert purge when CDTs for various hydrazines are examined with and without air present during hypergolic bipropellant reactions. Finally, some hypergols are hydroscopic and must be handled to minimize water vapor absorption. For systems such as these, a glove box purged with a dry gas, such as Argon, must be used during handling, along with an inert purge during the CDT measurements. Standard deviation for CDTs also improved once a purge was incorporated, as it sweeps the chamber clear of combustion products from the previous experiment.

Thus for accurate CDT measurement, contamination with water vapor or additional reactive pathways involving other oxidizers, such as oxygen must be controlled. A purge is a necessity for these cases.

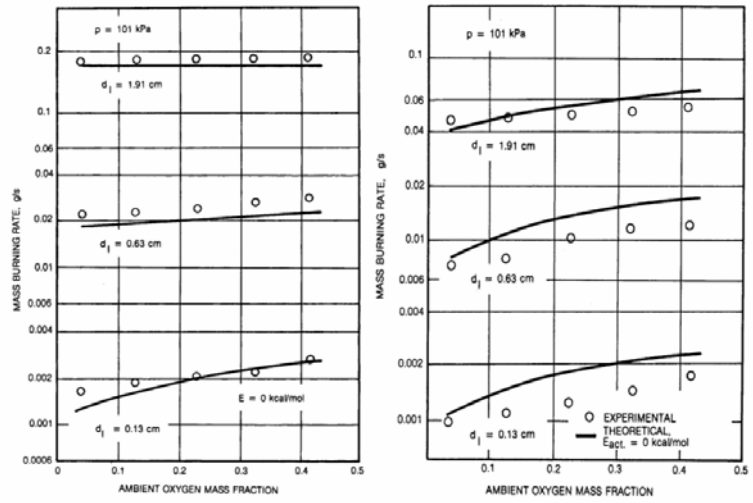

Figure 5: Hydrazine/Air combustion (left) and MMH/Air combustion (right) (Schmidt 2001)

1.3.5 Fuel Versus Oxidizer Lead

For the Laser Diagnostic Approach, droplet size was controlled by using precision hypodermic syringes and three foot long needles either controlled manually or by a positive displacement pump, such that a droplet of 0.07-

0.10 μL can be reproducibly created. It is also important to consider either fuel or oxidizer lead. For our technique the principal focus was on fuel lead as it minimizes the loss due to evaporation of the mixed oxidizer, typically red fuming nitric acid. In addition, the evaporation of dissolved N_2O_4 disrupts the timing system, thereby reducing resolution. Small droplets are also important when one considers safety associated with these compounds.

1.3.6 Safety

Hypergolic bipropellants are highly toxic and must be handled with extreme care. The toxic nature of these substances requires that certain precautions to be taken in order to limit the ramifications of an accident in a university setting. The first precaution taken was the use of high velocity exhaust vents. Combustion experiments as well as the handling of all chemicals were accomplished under high velocity exhaust vents.

The second measure taken to ensure safe experimentation was to use microliter volumes of all substances needed to perform combustion. Using Occupational Safety and Health Administration (OSHA) Permissible Exposure Limits (PEL) (defined as the concentration of a substance in the air based on an 8-hour time weighted average exposure), compound liquid densities and an approximate laboratory volume of 315 m^3 with all ventilators off gives the Maximum Volume of the compounds that could be utilized during this research as shown in Table 1 (Sax 1987). Maximum volume was obtained by multiplying the compound specific OSHA PEL by the volume of the room, then dividing by the liquid density of that compound. While these Maximum Volumes are within OSHA safety regulations, to further reduce the harmful effect of an accident, such as dropping and breaking a full syringe, the Working Volume of each substance was reduced to 25% of the Maximum Volume yielding a safety factor of at least 4. Thus, assuming a droplet size of approximately 7 μL, a Working Volume of 100 μL would allow for 14 drop-on-drop experiments to be performed without refilling the syringe.

Table 1: Safety Information for Common Reagents Used in Experimentation

Compounds	OSHA PEL (ppm)	OSHA PEL (mg/m^3)	Maximum Volume (mL)	Working Volume (mL)
Anhydrous Hydrazine (AH)	1	1.3	0.405	0.100
Monomethyl Hydrazine (MMH)	0.2	0.35	0.125	0.030
Red Fuming Nitric Acid (RFNA)	2	5	1.05	0.250
Dinitrogen Tetroxide	5	9	1.97	0.500

The third safeguard employed in creating a safe working environment was to provide the proper protective attire. Acid-proof aprons, laser-filtering safety goggles, latex gloves, and gas masks were worn during experimentation to reduce bodily harm caused by an accident. Another safety consideration was the use of a 3.28 M sodium hydroxide solution to neutralize oxidizer and fuel present after combustion experiments. The maximum volumes set forth by the safety regulations also put limitations on the experimentation. Operation of the combustor at steady state would require a greater volume of material than permissible in a university setting.

2.0 EQUIPMENT AND PROCEDURES

2.1.1 Drop-on-drop Measurements for Fast Reaction

Development of micro-liter droplets that match the bipropellant model can not be generated on demand. Instead, the method must be triggered by the fall of the droplet into the appropriate pool of the other component to initiate event timing. One of the most crucial aspects of successful drop-on-drop measurements is the initiation of the timing sequence.

Figure 6 shows one of three combustors developed during this research that are triggered by the falling droplet. To measure the ignition delay with the system, an Argon-Ion laser source is passed directly above a droplet of oxidizer within the combustor, shown in Figure 6. This is accomplished by raising the combustor or combustion chamber until the bottom edge of the Gaussian laser source is clipped by the top edge of the combustor. This also aligns the laser beam with the top surface of the oxidizer droplet.

The phototransistor shown in Figure 6, has a rise time of 2 μs, a spectral band pass from visible to IR, and can operate at voltages up to 30 VDC. The phototransistor is mounted in an optical mount, restricted by a pinhole aperture that limits the line-of-sight of the phototransistor to approximately 200 μm above the surface of the oxidizer pool. The phototransistor is positioned by a three axis micropositioner. The phototransistor is aligned with the laser/combustor plate by lowering the phototransistor until the laser signal dissipates. The phototransistor is then

raised until the signal to the detector is maximized. This alignment assures that the phototransistor is positioned just above the top edge of the combustor plate or liquid pool.

To conduct a fuel lead CDT experiment, once the combustion chamber was purged a small amount of fuel was placed into the combustor using a 250 μL syringe with a # 25 needle. After the fuel was placed into the combustor a single drop of oxidizer was dropped into the combustor using a 1.0 milliliter syringe or syringe drive pump with a special order 3 foot long # 22 needle. When a droplet falls from the hypodermic needle positioned directly above the center of the liquid pool on the combustor plate, the droplet falls through the path of the laser. The droplet falling through the laser disrupts the laser signal seen by the phototransistor. This disturbance of the signal triggers the recording of the digital storage oscilloscope (DSO). The DSO records the droplet falling through the laser just above the top edge of the combustor plate.

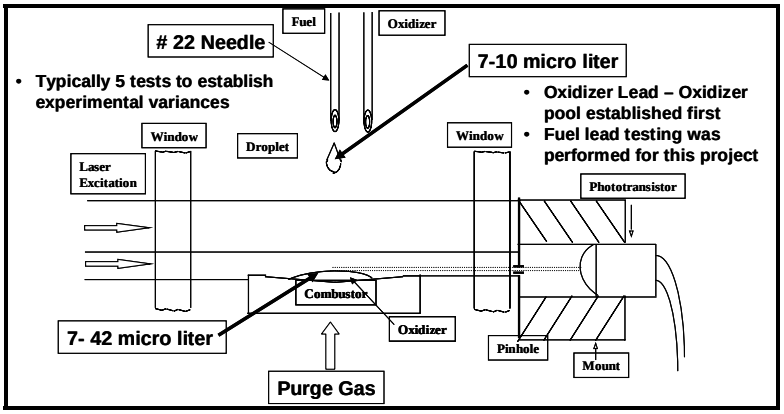

Figure 6: Droplet Timing with Purge Applied

To interface the droplet initiation to the events associated with the IDT/CDT measurements two separate phototransistor circuits are utilized. As shown in Figure 7, two phototransistors are required to monitor the chamber. In operation, phototransistor #1 monitors the laser beam intensity through a pinhole 200 μm in diameter, as described above. Phototransistor #2 monitors emission from the combustor through a band pass filter that eliminates scatter light from the Argon-Ion laser source. The filter is necessary due to the extreme sensitivity of this phototransistor throughout the visible and near infrared spectrum. A series of concentrating optics are used to collect the flame emission, as shown in Figure 8. The focusing optics restricts the view of the flame by the phototransistor to a region approximately ¼ inch in diameter, directly above and centered on the combustor.

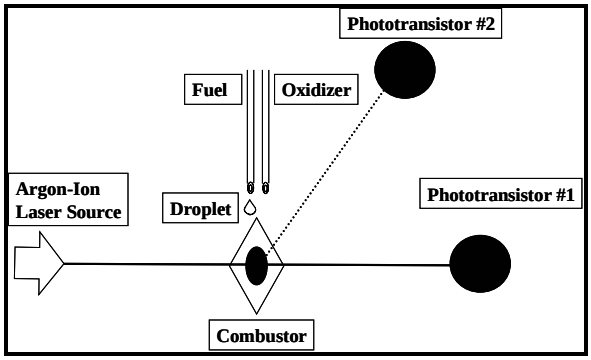

Figure 7: Phototransistor Timing Circuits

A precalculated amount of oxidizer is placed onto the combustor through a hypodermic needle as shown in Figure 6. Then a fuel droplet of known volume is discharged from the second hypodermic needle positioned approximately 1.5 cm above the oxidizer. This droplet passes through the laser beam and attenuates the response of phototransistor #1, which will be seen as a decrease in signal on channel 1 of the DSO. This marks the moment of contact between fuel and oxidizer. Later, a vapor phase above the fuel and oxidizer pool ignites, and the flame sensed by phototransistor #2, shown in Figure 7. Channel 2 of the DSO, measures the output from phototransistor #2. The time lag between these two events is a direct measurement of the ignition delay.

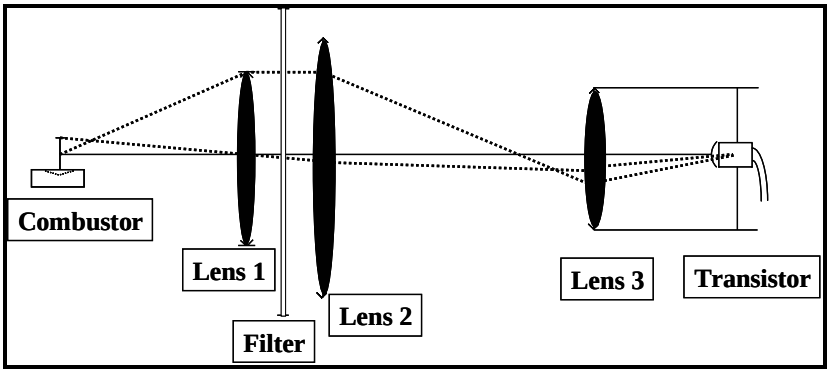

Figure 8: Optical Orientation for Channel 2

2.1.2 Digital Storage Oscilloscope

To resolve very rapid events into the microsecond region, the laser diagnostic system described earlier by Farmer (1997) and Mays (1998) was modified to improve CDT measurement accuracy, detector sensitivity, and chemical analysis (Hampton et al. 2004a). Accuracy was improved by adding a Digital Storage Oscilloscope (DSO) with true TTL level external trigger capabilities, sensitivity by incorporating faster components in both detectors.

The most critical aspect to the Laser Diagnostic System (LDS) is the DSO which must have a "real-time" TTL level trigger. Many DSO's have an external trigger; however, their speed is typically not a benchmark of the DSO and varies greatly from manufacturer to manufacturer. In the early stages of this project, DSO's from many vendors were reviewed and the triggering speed discussed with their technical departments to understand their external triggering speed and voltage, and included HP, LeCroy, Tektronix, etc,. Of these, only Tektronix had an external TTL level triggering speed that was virtually "real-time" relative to events we wished to measure. Their external triggering speed was quoted by a technician at $\cong$ 60 nanosecond; however since it was not a bench mark component it could not be guaranteed without significant testing.

A Tektronix representative conducted a series of trigger delay time measurements on 11 separate TDS5000 series DSO production models. They measured an average of 50.8 nanoseconds with a standard deviation of 1.33 nanoseconds, well within the 60 nanoseconds needed. Based on this analysis, a Tektronix model TDS 5104 was purchased with 1 and 1.5 GHz active probes to handle the voltages on the two detectors and WaveStar software for oscilloscopes. Our model TDS5104 has a fully programmable trigger that can trigger both laser pulses and the two optical multi-channel analyzers. The TDS5104 was also equipped with WaveStar on-screen oscilloscope analysis software which provides enhanced analysis capability for the determination of the CDT.

The on screen analysis software permits a greater degree of accuracy since measurements are made directly on the computer monitor, rather than on paper printouts used previously (Mays 1998). Figures 9 and 10 are representative CDT spectrum on paper printouts and using the TDS5104, respectively. Using this figure and its on screen cursors, point C (point where gas is being evolved) can be quickly determined, while the second cursor is placed at the point where detector 2 detects emission from the combustion zone. The software measures the distance between these two cursors, displaying the difference in the upper left corner in this case. In Figure 10, the CDT is measured as the time between the appearance of gas at point C and combustion at point D as 904 μs.

Previously, data were recorded on small dot-matrix printouts from a LeCroy 9360 DSO (Mays 1998). The ignition and chemical delay times had to be physically measured from the plots, which magnified human error. With the addition of the Tektronix TDS 5104 DSO, the data analysis is measured on the computer monitor minimizing human error and permitting faster and more precise data analysis. A comparison of the paper printout from the Tektronix TDS 5104 DSO of a water drop test from a hypodermic needle was measured both manually and automatically. Manually an average result of 4.4 msec was measured while the automated method measured 4.6740 msec (Hampton et al. 2003). This resulted in a 5.9% measurement error. This addition to the system dramatically increased measurement accuracy, reproducibility and further enhanced the ability to identify atmospheric and mixture effects in hypergolic bipropellant systems.

Figure 10 shows an example of data obtained during a typical CDT experiment. The upper line represents the Argon-Ion Laser signal observed by Phototransistor #1, while the lower line is that of the signal received by Phototransistor #2. The section between points A and B represents the oxidizer drop falling through a narrow portion of the Argon-Ion Laser as described previously. By working with microliter volumes, the reaction delay caused by mixing is minimized, therefore the time between points B and C is the liquid reaction time (LRT) where

the oxidizer and fuel are reacting, potentially forming intermediates. At point C, a spontaneous decomposition occurs with the evolution of vapor causing a decrease in the output of Phototransistor #1. The resulting ignition is sensed by Phototransistor #2. Since all signal data is stored electronically, the oscilloscope software can measure the time between cursors placed visually at points C and D with the dX representing the CDT as shown in the upper left corner of Figure 10.

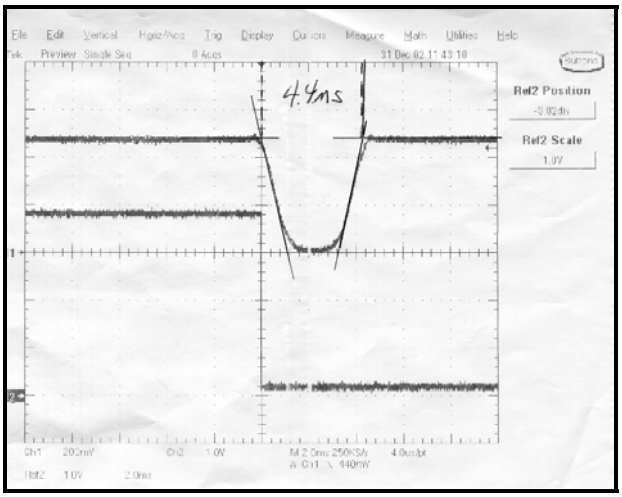

Figure 9: Paper Test for Determining CDT

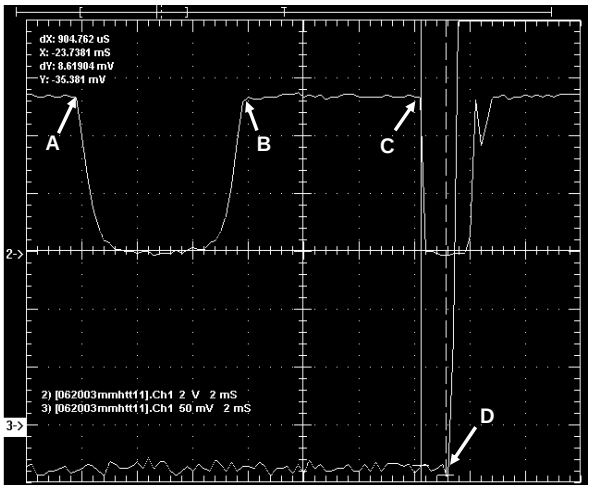

Figure 10: MMH/RFNA data at a Fuel / Oxidizer Ratio of 1/3 by Volume

2.1.3 Ceramic Heating Stage Evolution

The combustion plate initially began as a conically shaped stainless steel platform, made from 304-stainless steel, and shown in Figures 6 and 11. Previous drop-on-drop combustion experiments were conducted on this stage in order to obtain isothermal operation. It was noticed, however, that certain fuels behaved differently compared to others. Based on the assumption that the stainless steel plate was acting as a heat sink and removing heat from the combustion reaction, it was concluded that performing experiments on a ceramic combustion plate might resolve this problem. The ceramic combustion plate, shown in Figure 12, was used to perform combustion experiments more adiabatically. However, when combustions experiments were successively performed it was noticed that the chemical delay times were becoming faster, as shown in Table 2 below.

Table 2: Example of CDT's for Successive Combustions on a Ceramic Plate

Test #	CDT (ms)
1	14.4211
2	14
3	14.4662
4	14.6316
5	12.3684
6	11.3158
7	9.8421

It was determined that the heat of the combustion was introducing heat into the ceramic plate and causing the fuel lead to heat before the oxidizer could make contact. The successive combustions were performed quickly enough such that the heat introduced into the ceramic plate could not dissipate before the next experiment was performed. From this it was concluded that controlling the temperature of the ceramic plate would in turn control the temperature of the fuel lead. The ability to control the temperature of the fuel lead would allow for chemical delay time measurements to be taken at higher temperatures and obtain information on the effect of preheat temperature on chemical delay time. The current heated combustion plate, shown in Figure 13, consists of a ceramic plate that is thermally controlled by an in-house designed electric heater.

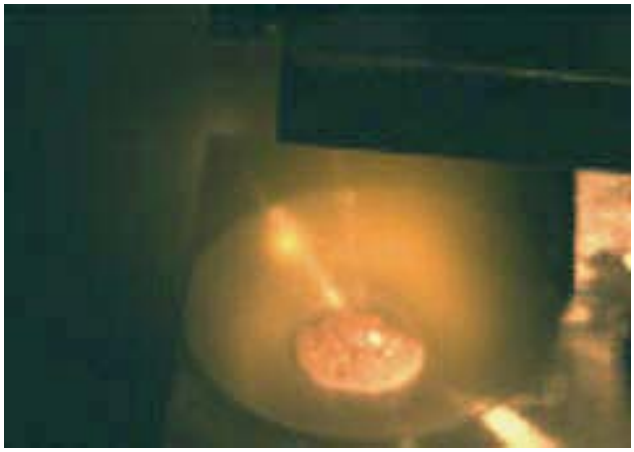

Figure 11: Stainless Steel Combustion for Isothermal Operation

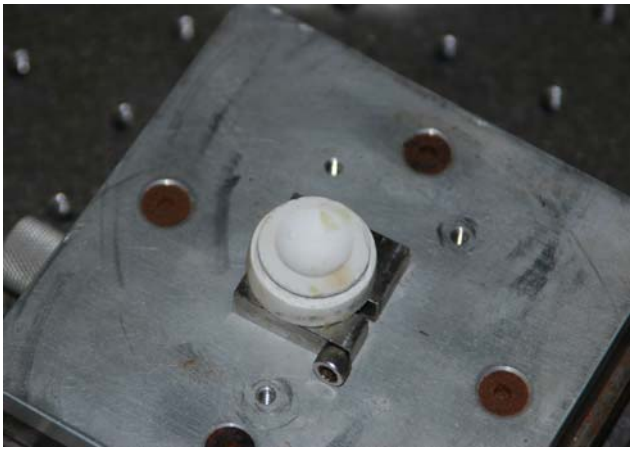

Figure 12: Ceramic Combustor for Adiabatic Combustion

Figure 13: Thermally Controlled Ceramic Combustor

The stainless steel combustor plate used with previous approaches was replaced with a ceramic heating stage. The ceramic combustion plate shown in Figure 14 was made from an alumina closed-bottom ceramic tube. The end of this ceramic tube, approximately 0.75 inches inside diameter and 0.125 inch wall thickness, was cut using a diamond saw. The wall thickness at the bowl base was thinned to approximately 0.03125 inches to improve thermal response as discussed later. A 1 inch piece of ceramic tubing was threaded with 12 threads per inch and placed on top of the inverted ceramic bowl. A second ceramic tube 0.125 inches in diameter was cemented inside the threaded tube to the bottom of the ceramic bowl at the thinned-out point using Saueresien Insultemp Cement No. 10. The space between the 0.125 inch diameter tubing and the threaded tubing was filled with cement to secure both tubes to the inverted ceramic bowl. An open-junction Type J thermocouple was secured inside the 0.125 inch diameter tubing to record temperatures of the preheated liquid. Since the thickness of the bowl base had been thinned, the temperature read by the thermocouple was as close to the temperature of the liquid placed within the bowl as possible without placing a thermocouple directly in the liquid. The corrosiveness of the liquid compounds being placed inside the ceramic bowl prohibited the placement of an open junction thermocouple directly in the liquid.

The heater consisted of a 0.015 inch diameter copper-nickel (Constantan) resistive wire wrapped in the grooves of the threaded tube and cemented in place. The resistive wires were connected by copper lead wires to a 6 volt power supply. The thickness of the wiring limited the maximum current to approximately 2 amps. The available power produced a temperature ranging from room temperature to approximately 350 ˚F/176 ˚C. The temperature of the combustion platform was changed by adjusting the amount of applied power from the power supply. Each end of the wiring was covered with a ceramic tube to prevent any contact with corrosive chemicals, see Figure 13. The height of the heating stage, Figure 14 was adjusted to maintain the same configurations as the original stainless steel version, Figure 6.

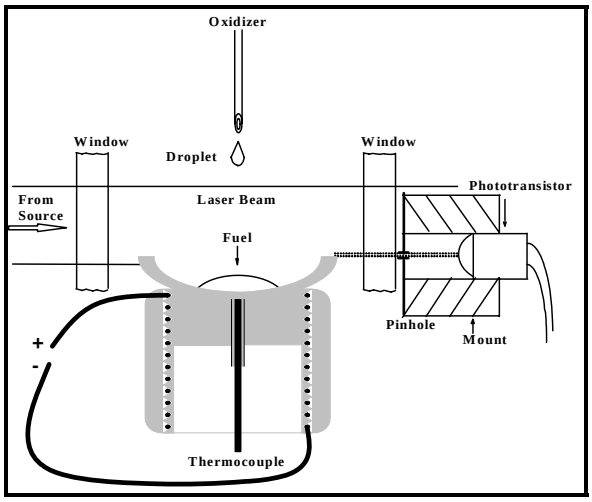

Figure 14: Heating Stage Schematic

2.1.4 Liquid Phase Reaction Temperature

In order to determine the liquid mixture temperature during the reaction between Anhydrous Hydrazine and Red Fuming Nitric Acid, it was necessary to make additional modifications to the combustion chamber. A removable open junction type K thermocouple was attached to the combustion chamber. A type K thermocouple has an operation range of -269 to 1260 C. The thermocouple was constructed of 0.005-inch diameter PFA-Teflon coated Alumel and Chromel wires placed within a three-inch piece of two-hole ceramic tubing. The portion of the thermocouple that was placed in the liquid mixture was fashioned into a loop in order to create the maximum number of reading points at different locations, since the temperature obtained is an average of all points where the two metals are in contact. Ceramic tubing with two holes served a dual purpose. Since the tubing was ceramic, it did not have the heat sink properties of metal or glass but still retained the high electrical resistance. Using tubing with a separate hole for each wire ensured that neither unsheathed wire would come into contact with the other and result in an additional reading point outside the liquid regime. Any reading outside the liquid regime, in the flame region for example, would give inaccurate temperature measurements for the liquid phase reaction.

The thermocouple was connected to an IOtech DaqBook/200 16-bit Data Acquisition System with an Enhanced Parallel Port installed and a DBK-19 High Accuracy Thermocouple Card. This system was used to collect temperature versus time data using DaqView software to interface with the DaqBook/200. The DaqView software was configured to collect 10,000 samples per second for a period of 3 seconds to completely capture the resulting phenomena. Data collection was triggered manually and stopped automatically once 3 seconds had elapsed.

2.1.5 The Overall Laser Diagnostic System

The entire operating system was designed to study the reaction rates and mechanisms of hypergolic bipropellants are shown in Figure 15. The combustion chamber, supporting systems, and diagnostics were designed and assembled as detailed in a recent publication (Farmer et al. 2002). The laser source currently employed for the chemical delay measurements is an Argon-Ion laser. A Tektronix Digital Storage Oscilloscope was used to measure the ignition and chemical delay times. The outputs of all system components were fully interfaced to computers.

The combustion chamber is shown in Figure 16. The body and flanges were machined from 304-stainless steel. The chamber itself can be sealed and pressurized to hold a flowing, inert gas or vacuum. All test results presented in this report were performed at atmospheric pressure in air or inert gas.

The chamber contains eight side ports. One port supports a linear positioner that is used to align any one of three combustors previously described with the laser(s). Another port provides feed through of hypodermic needles connected to Cole-Parmer digital syringe pumps to inject the fuel and oxidizer. There is also a port for temperature and pressure monitoring of the chamber. The remaining ports hold high quality optics for laser diagnostics at the appropriate wavelength.

Currently, the combustion system supports ignition time delay studies between liquid fuel and oxidizer under various atmospheres but can be modified to support a host of fuel/oxidizer combinations including gels and liquid/solid propellants for hybrid systems.

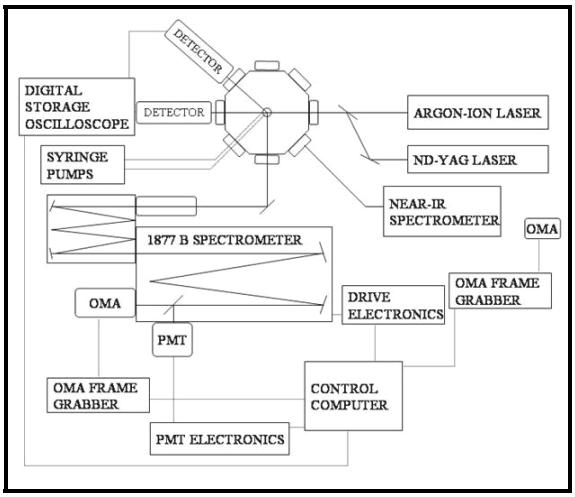

Figure 15: Overview of the Entire System

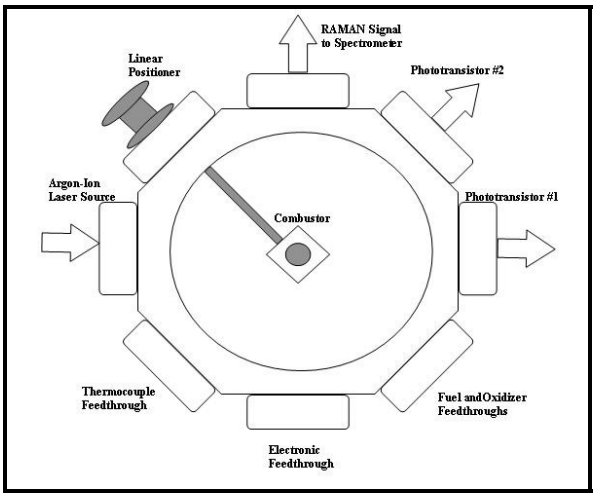

Figure 16: Top View of the Combustion Chamber

2.1.6 High Speed Video

At the time of the proposal, a EG&G model 4256 1000 fps camera was to be used to collect images to a pair of Dipix frame grabbers installed in a IBM PC. Unfortunately the system failed. The University agreed to purchase a high speed color camera for this project. The camera is an EPIX BASLER A504kc color camera combined with a PIXCI-CL3SD-A504kc frame grabber. The camera comes with all hardware and software installed and tested in a P-4 IBM PC. The software provides camera controls including exposure; frame rate, and region of interest, the ability to capture and display image sequences and individual images saved or printed as well as image processing, analysis, and measurement features. The camera came equipped with a TTL-level trigger input conversion module which allows the camera to be triggered by the Digital Storage Oscilloscope (DSO). With 1 GB of memory the camera can operate between 500 fps and 8000 fps depending upon window size.

With the purchase of a high speed color camera subjects such as droplet dynamics, explosion locations, droplet-droplet interactions, minimizing vortex ring effects on the combustion, and optimizing reactor dimensions can be addressed with a better understanding of what is occurring during the combustion. An example of a frame from the high-speed video can be seen in Figure 11. High-speed video has been included in many presentations, contractor meetings and papers. This camera further defined events occurring during hypergolic bipropellant combustion.

3.0 RESULTS AND DISCUSSION

3.1.1 Effects of Atmospheric Conditions

In section 1.3.4, the importance of a system purge to CDT measurements was discussed. This section further expands upon the importance of the purge during hypergolic bipropellant reactions, which atmospheric techniques, such as Broatch (1950) and others do not consider.

The CDT of pure components; Anhydrous Hydrazine, Mono-Methylhydrazine (MMH), and Unsymmetrical Dimethylhydrazine (UDMH) reacted with red fuming nitric acid (RFNA) on a molar and mass basis were compared to mixtures of the same species under both air and inert atmospheres. Figure 17 shows a summary of the Chemical Delay Time results for all three fuels studied on a molar and mass basis. Referring to Figure 17, UDMH demonstrated no significant difference in CDT under Argon or atmospheric air. Hydrazine showed only about a 4 percent difference in CDT measurements between Argon and atmospheric air. For MMH there was a 23 percent maximum difference in CDT between atmospheric air and Argon gas. For hydrazine and MMH all results showed that CDT measurements conducted under atmospheric air were faster than those conducted under Argon.

Figure 17 shows that the molar reaction rate for hydrazine exceeds that of MMH, even though the CDT for hydrazine is slower. This is due to the higher density and lower molecular weight of hydrazine. Thus, more moles of hydrazine are consumed per second than MMH. In terms of mass, MMH appears to have the higher reaction rate than Hydrazine, also shown in Figure 17. The reason for this disparity is related to the density, surface tension, and molecular weight of each species that consequently controls the number of moles of fuel within each drop. MMH has at least one major difference from other hydrazines studied; it is a highly asymmetric polar compound, which may be a contributing factor to the enhancements observed. Figure 17 shows that MMH either desires or can utilize more atmospheric oxygen than either Hydrazine or UDMH.

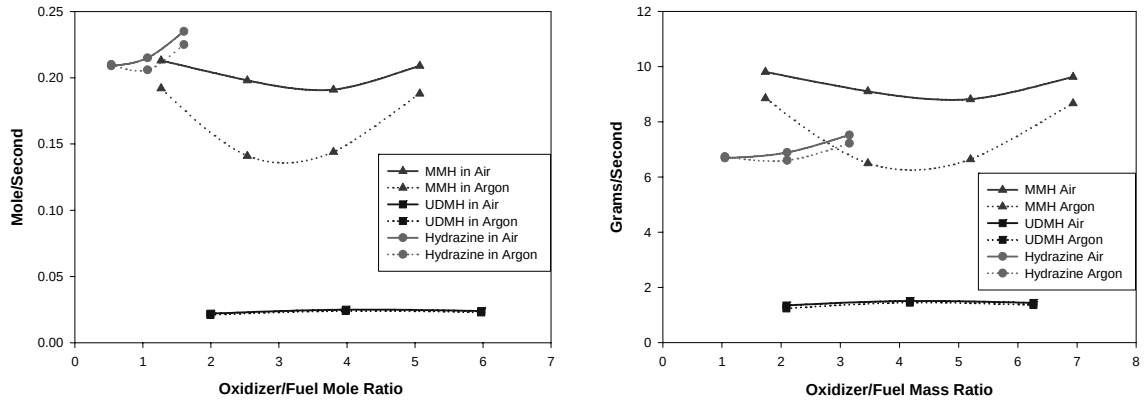

Figure 17: Comparison of Molar and Mass Reaction Rate for Hydrazines/RFNA

An important issue is raised in Figure 17 is classical combustion studies view reaction rates in terms of a mass rather than a molar basis. The traditional method of depicting combustion rates is by mass, not moles, according to Schmidt (2001). However, from Figure 17, it can clearly be seen that on a molar basis, hydrazine reacts at the same molar rate or faster than MMH, while on a mass basis MMH is faster that hydrazine. From this observation, it was deemed that all future experiments should be conducted on a molar basis and converted to mass. Having characterized the effect of atmospheric air and Argon gas on representative fuels, the next step was to determine the effect of carbon/nitrogen ratio on chemical delay. Specific details on this technique can be found in Hampton et al. (2004a).

3.1.2 Effect of Carbon/Nitrogen Ratio

In our previous studies, Hampton et al. (2003), the issue of mixed hydrazines and their effect on CDT was presented. This work showed that 50 volume percent UDMH added to hydrazine decreases the CDT by 71% relative to ideal mixing as the reference point, making this mixture as reactive as MMH/RFNA as shown in Figure 18. Thus, the presence of carbon influences the CDT, clearly showing that carbon is important to the reaction mechanism. It is also obvious that too much carbon or no carbon at all slows the reaction. Therefore it was it was beneficial to further detail the importance of the carbon to nitrogen ratios in hydrazine mixtures.

Based on the fact that the CDT for Hydrazine/UDMH mixtures differed from what would be expected if ideal mixing was assumed, additional experiments were conducted to determine the CDT for Hydrazine/MMH mixtures. Mixtures of Hydrazine/MMH were varied with molar percentage of MMH from 0 to 100% which resulted in a set of mixtures that varied the C/N atom ratio from 0 to 0.5. For mixtures with C/N ratios from 0.5 – 1, the addition of UDMH was necessary to increase the C/N atom ratio. Previous data contained only Hydrazine/UDMH mixtures with a range of 0 – 1 for C/N atom ratios. Referring to Figure 18, Hydrazine/MMH mixtures were investigated in the range of 0 – 0.5 C/N, while tertiary mixtures of Hydrazine/MMH/UDMH were investigated in the range of 0.5 – 1 C/N. This addition of MMH to Hydrazine/UDMH mixtures resulted in improvements in the CDT when the asymmetric polar compound was included in the mix as shown in Figure 18. Thus, greater performance across the entire domain was achieved by controlling tertiary mixtures to maintain the C/N atom ratio at the desired level. With the use of tertiary mixtures the actual toxicity of a given hydrazine was reduced from that of the pure component. Actual mixture data used to create Figure 18 is shown in Table 3, below.

There are several important aspects of Figure 18 that must be recognized; the first is that previous data, triangles in Figure 18, are for mixtures of only Hydrazine/UDMH reacted with RFNA, while the new data, circles in Figure 18, are for mixtures of Hydrazine/MMH reacted with RFNA for C/N of 0 – 0.5 and Hydrazine/UDMH/MMH reacted with RFNA for C/N of 0.5 – 1.0. For the C/N ratio in the range of 0 – 0.5 the addition of MMH to Hydrazine did not change the CDT measurements significantly from the addition of UDMH to Hydrazine. Another important fact is that for pure Hydrazine (C/N = 0), pure UDMH (C/N = 1), and pure MMH (C/N = 0.5), the CDT results are within the previous data range and features less relative error. Therefore, the overall precision of the technique has been increased with the modifications in the experimental apparatus as well as CDT measurement techniques described in previous sections.

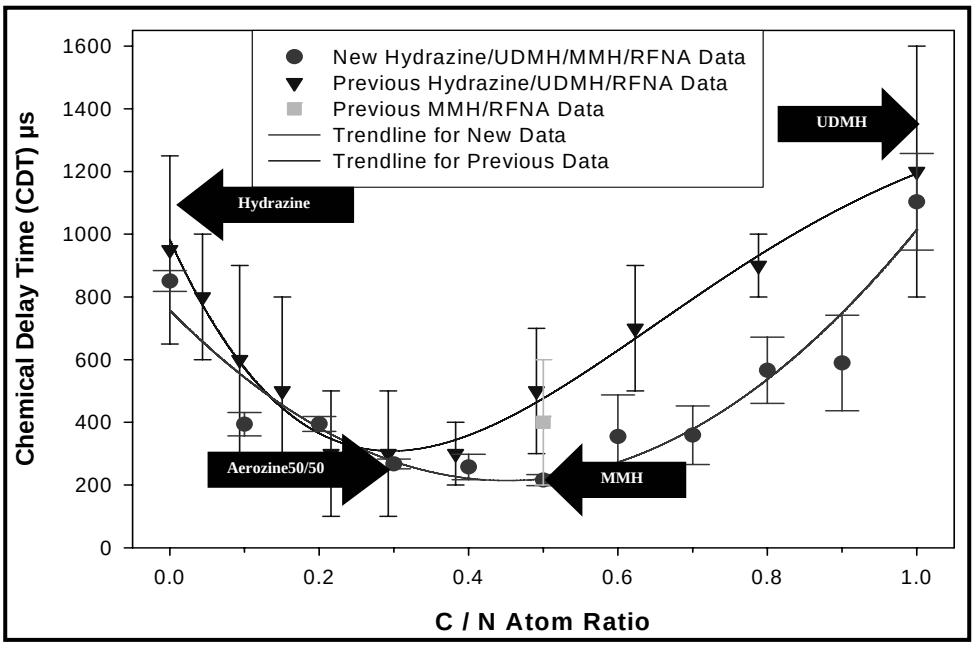

Figure 18: Comparison of CDT with Different C/N Atom Ratios

Table 3: Molar Compositions and C/N Ratios for Data in Figure 18

New Data				Previous Data		
	Molar Percent				Molar Percent	
C/N Ratio	Hydrazine	UDMH	MMH	C/N Ratio	Hydrazine	UDMH
0.00	100	0	0	0.00	100.00	0.00
0.10	80	0	20	0.04	95.61	4.39
0.20	60	0	40	0.09	90.64	9.36
0.30	40	0	60	0.15	84.96	15.04
0.40	20	0	80	0.22	78.40	21.60
0.50	0	0	100	0.29	70.76	29.24
0.60	20	40	40	0.38	61.74	38.26
0.70	20	60	20	0.49	50.92	49.08
0.80	10	70	20	0.62	37.70	62.30
0.90	5	85	10	0.79	21.19	78.81
1.00	0	100	0	1.00	0.00	100.00

The data point shown as a square in Figure 18 was previously measured by Mays (1998) at 0.4 $\pm$ 0.2 milliseconds, which represents 8 measurements at an oxidizer to fuel mass ratio of 1.4. This measurement was later confirmed by Anderson (1999a) of Talley Defense Inc. for the TRW Corporation using high-pressure impinging jet tests of MMH with IRFNA for equal volumes of MMH and IRFNA. Only one MMH/IRFNA experiment was conducted by Talley and the oxidizer to fuel ratio could not be directly determined (Anderson 1999a, 1999b). The modified laser diagnostic system discussed in previous sections has produced higher resolutions and increased precision as shown in Figure 18. The results at a C/N of 0.5 represent 6 measurements with a CDT of 0.2 $\pm$ 0.02 milliseconds at an oxidizer to fuel mass ratio of 1.9.

Also, the differences in CDT for a C/N ratio from 0.5 – 1.0, shown in Figure 18, should be noted. For the range of C/N ratio of 0.5 – 1.0 there is on average about a 46% decrease in CDT for data collected using ternary solutions compared binary solutions. This is due to the fact that the binary data did not contain MMH. This suggests that adding an asymmetric polar compound, such as MMH, could reduce the CDT for other hydrazines or azides.

Because of the decrease in CDT for the ternary mixtures of Hydrazine/MMH/UDMH with in the C/N atom ratio of 0.5 – 1.0, binary mixtures of MMH/UDMH should be investigated with this range.

3.1.3 Oxygenation of Hydrazine/UDMH Mixtures

It is known that too much oxygen added to the fuel can have a detrimental effect on ISP. This oxygen can react with the fuel by either crossing the fuel/oxidizer interface or added directly to the fuel to provide an internal source of oxygen. It was shown previously that the presence of atmospheric oxygen during the combustion greatly effects MMH/RFNA reactions and has only a slight to no effect for Hydrazine/RFNA and UDMH/RFNA reactions (Hampton and Smith 2004).

Pure Methanol was tested with RFNA and was found to not be hypergolic. At low Methanol concentrations (5%) in hydrazine the mixture was hypergolic. However at high concentrations (>10%), contact with RFNA produced heat that was absorbed by the rapidly evaporating Methanol and not enough heat remained to spontaneously ignite the mixture. Additions of Methanol to UDMH produced similar results. The reactions with pure Hydrazine and UDMH mixed with Methanol produced two different phenomena. At low Methanol concentrations (<5%) upon contact with RFNA both Hydrazine and UDMH produced two different combustion phenomena. During several tests, as the Methanol evaporated, the remaining pool of hydrazine ignited, with a flame similar to normal hypergolic combustion of hydrazines/RFNA, triggering an explosion of the now premixed Methanol/air mixture above the initial combustion zone. However, at high concentrations (>10%) of Methanol with pure Hydrazine and UDMH, contact with RFNA produced an immediate explosion which completely filled the combustion chamber with smoke, typical of incomplete combustion.

Mixtures of UDMH, Hydrazine, and Methanol at a constant C/N ratio of 0.3 were reacted with RFNA to determine if oxygenating Hydrazine/UDMH mixtures with methanol would decrease the CDT, shown in Figure 19. The C/N ratio of 0.3 was chosen because earlier CDT measurements of Hydrazine/UDMH mixtures, outlined in section 3.1.2, showed that the minimum CDT occurred 50 % Hydrazine in UDMH by volume, which results in a C/N of 0.3. For each Hydrazine/UDMH/Methanol mixture the concentrations of Hydrazine and UDMH were adjusted so that the resulting C/N atom ratio would be 0.3. By maintaining the C/N ratio constant at 0.3, on an atomic scale, the only difference between the Hydrazine/UDMH mixtures without Methanol and those with Methanol was the addition of oxygen and hydrogen atoms to the mix.

Figure 19 clearly shows that the CDT measurements for Hydrazine/UDMH/Methanol mixtures are constant with only slight fluctuations. Thus, only a very small amount of Methanol can be added to the Hydrazine/UDMH mixtures. At the higher concentrations, two separate phenomena, described above, often occurred. Methanol evaporation and the resulting explosion triggered by hypergolic ignition suggests that mixtures with higher contents of Methanol should be run at high pressure to prevent rapid evaporation of the Methanol thus permitting greater contact time between the hypergolic bipropellant mixtures.

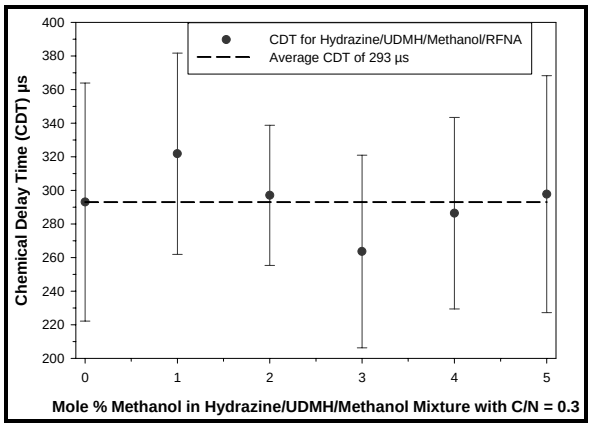

Figure 19: CDT for Hydrazine / UDMH / Methanol / RFNA Mixtures

3.1.4 Oxygenation of MMH

Previous experiments conducted under an Argon atmosphere or under atmospheric air, outlined in section 3.1.1, showed that MMH needs or can use more oxygen during the combustion with RFNA (Hampton and Smith 2004). This suggested that MMH could benefit from the addition of an oxygenating agent. Therefore, MMH was oxygenated with Methanol up to 45 mole % and reacted with RFNA. Mixtures above 45 mole % immediately

exploded similar to that discussed above for Hydrazine and UDMH. CDT experiments for the range of 0 – 30 mole % Methanol were conducted with fuel lead while experiments in the range of 35 – 45 mole % Methanol were performed with oxidizer lead. Fuel lead describes the experiment when a known amount of fuel was placed within the combustor plate and a droplet of oxidizer was aspirated onto the fuel. In oxidizer lead, a known amount of oxidizer was placed within the combustor plate and a droplet of fuel was aspirated onto the oxidizer. The method of experimentation was changed at 30 mole % Methanol from fuel lead to oxidizer lead in an effort to suppress explosion, as described above. For oxidizer lead in the range of 35 – 45 mole % Methanol, explosion seldom occurred. Having to switch between fuel and oxidizer leads to prevent explosion again suggests that higher pressure operation could suppress explosion causing stable combustion.

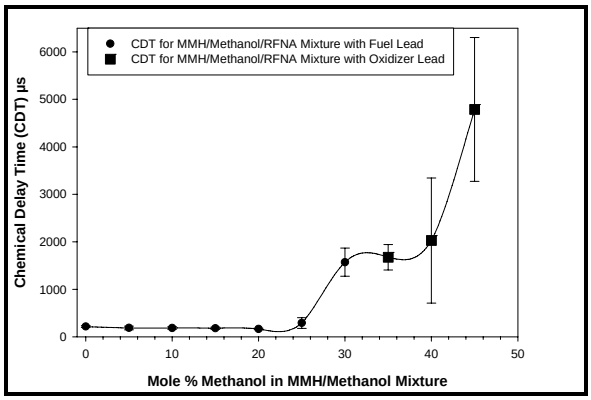

Figure 20: CDT Measurements for MMH/Methanol Mixtures

Figure 20 shows the resulting CDT measurements for the MMH/Methanol mixtures reacted with RFNA. In Figure 20 the two distinct regions, fuel lead (0 – 30 mole % Methanol) and oxidizer lead (35 – 45 mole % Methanol) are clearly discernable. The large errors at the higher concentrations are attributed to combustion instabilities associated with hypergolicity and Methanol evaporation. Figure 21 expands on Figure 20 and shows the CDT measurements for 0 – 25 mole % Methanol. The CDT for pure MMH has been benchmarked on Figure 21 by the horizontal line added to the figure. Notice that the CDT for MMH/Methanol mixtures actually decreases from that of pure MMH up to compositions of 20 mole % Methanol. From Figure 21, mixtures with compositions of about 23 mole % Methanol produce the same average CDT as pure MMH.

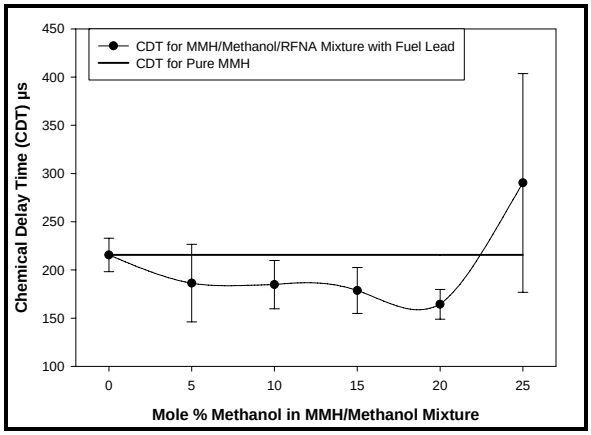

Figure 21: CDT Measurements for 0 – 25 Molar % Methanol in MMH

Adding Methanol to MMH decreased the CDT for all compositions tested up to 20 mole % Methanol as shown in Figure 21. Beyond the 20 molar % Methanol the CDT significantly increased. This suggests that the addition of oxygenating compounds to asymmetric polar amines or azides could reduce the CDT. Another important effect of oxygenating MMH with Methanol is the reduced toxicity of the MMH/Methanol mixtures compared to pure MMH. Further investigations into the effects of oxygenating hydrazines and azides may reduce CDT and toxicity.

When the MMH/Methanol mixtures were prepared for CDT measurements, the solutions would heat slightly. Since both Methanol and MMH are polar compounds, and polar mixtures often produce excess thermodynamic properties, a series of experiments were conducted to determine if both volume change, heat of mixing, and viscosity changes also occurred for this system. Previously published papers, Hampton et al. 2004b and Hampton and Smith, 2005 presented data on the various physical properties of mixing of MMH and Methanol. These will not be discussed here, with the exception of the volume and viscosity changes upon mixing

3.1.5 Possible Intermediate Specie in the MMH/Methanol System

Figure 22 below shows both the molar volume change on mixing and the viscosity change on mixing, referenced to the pure components at temperature and pressure of the system. For this figure, no single function would adequately reproduce the data. These data were therefore deconvoluted to find the best two peaks that when combined reproduced the original data. Two peaks typically indicate the presence of two phases, such as seen in immiscible liquid/liquid systems. However, for the MMH/Methanol system, the components are totally miscible in all proportions. It must be that both thermodynamic and transport phenomena influence the overall combustion in this system. Clusters or coordinating complex formations due to hydrogen bonding associated with the non-ideal solution behavior weakens the bond energy permitting the observed decrease in the CDT below 23 mole% Methanol. It is known that pure Hydrazine forms a hydrate with water through hydrogen bonding; however, no references could be found for similar compound formations with Methanol. Hydrate formation in either MMH or UDMH is also unknown. Experiments in this laboratory have shown that all three hydrazines are miscible in both water and Methanol. The non-ideal thermodynamic behavior between MMH and Methanol has been experimentally documented in this report. This might explain the presence of the first peak, while the second deconvolution peak represents the excess property resulting from further mixing.

Three distinct regions are apparent in Figure 22 when lines are drawn through the maxima and minima of the convoluted results. Region I produced stable combustion, region II showed meta-stable combustion behavior, while region III produced micro-explosions or was not hypergolic. Region I maximum is approximately 25 mole % Methanol, at which concentration, 3 moles of MMH would be hydrogen bonded with 1 mole of Methanol.

It is clear that the non-ideal solution thermodynamics greatly influenced the overall result for MMH/Methanol, since both Hydrazine and UDMH readily dissolved Methanol without significant changes in their physical or combustion behaviors. Though not shown here, heat of mixing data produced a similar trend to that of Figure 22. Heat of mixing data also required two peaks to deconvolute the result.

Based on results reported in the next section, it is also possible that an intermediate specie is formed that is far more reactive with RFNA than pure MMH.

3.1.6 Effect of Temperature on Chemical Delay Time

The procedure used to determine the effect of temperature on chemical delay time was similar to those described in earlier sections with one addition. To determine the temperature effect on the CDT of hypergolic bipropellants, it was first necessary to determine the temperature range for each particular hypergol. Each fuel has a different boiling point, establishing its higher endpoint, while the lower endpoint was set by the room temperature, approximately 20 ˚C. To conduct a CDT experiment, the thermally controlled ceramic combustor was first set to a specific temperature by adjusting the applied power.

The pure components tested in these experiments were: Anhydrous Hydrazine, MMH, UDMH, and several fuels under development by AMRDEC and two private companies Ogden Engineering and 3-D Research Corporation. The Chemical Delay Times of these fuels were studied at different temperatures in order to quantify the effect of temperature. Tables 4-7 show the results of these temperature studies. The temperature range for Hydrazine was larger than that of the fuels developed by the U.S. Army, but exhibited a much larger percent decrease in CDT. The CDT for Hydrazine, shown in Table 4, is about 620 μs just above room temperature but decreases significantly to 45.4 μs as it approaches its boiling point, consistent with a 92 percent decrease in CDT. While most of the fuels exhibited at least some decrease in CDT, one in particular experienced the opposite response to increase in temperature. Across the temperature range studied for UDMH, CDT increased from approximately 1.1 ms to just below 2.9 ms, constituting a 167 percent increase in CDT. This may have resulted from using a constant F/O ratio for all fuel studies. UDMH may have a higher oxidizer demand as temperature increases and should be a topic for further study. Table 6 shows a decrease in CDT for MMH from 546 μs to 255 μs across a temperature range of 44 K, giving the smallest change in CDT of the fuels tested of approximately 53 percent.

In order to compare the performance of these fuels, temperature change studied, initial CDT and average change in CDT per degree K are shown in Table 7. Since each fuel was tested over a slightly different temperature range, a relative measure of the average change in CDT per degree Kelvin provides the best comparison. As would be

expected from a benchmark fuel such as MMH, it experiences not only the smallest initial CDT (546 μs) for this F/O ratio, but also the smallest CDT change per degree Kelvin (6.56 μs/K). Hydrazine exhibits only a slightly greater CDT dependency on temperature (7.99 μs/K), while UDMH had a CDT that is greatly affected by changes in temperature, approximately 52, 132, and 161 μs/K, respectively. It is obvious that the percentage difference in not only the room temperature CDT but also the average CDT change per degree K of UDMH greatly exceeds that of the benchmark bipropellant MMH/RFNA by several orders of magnitude.

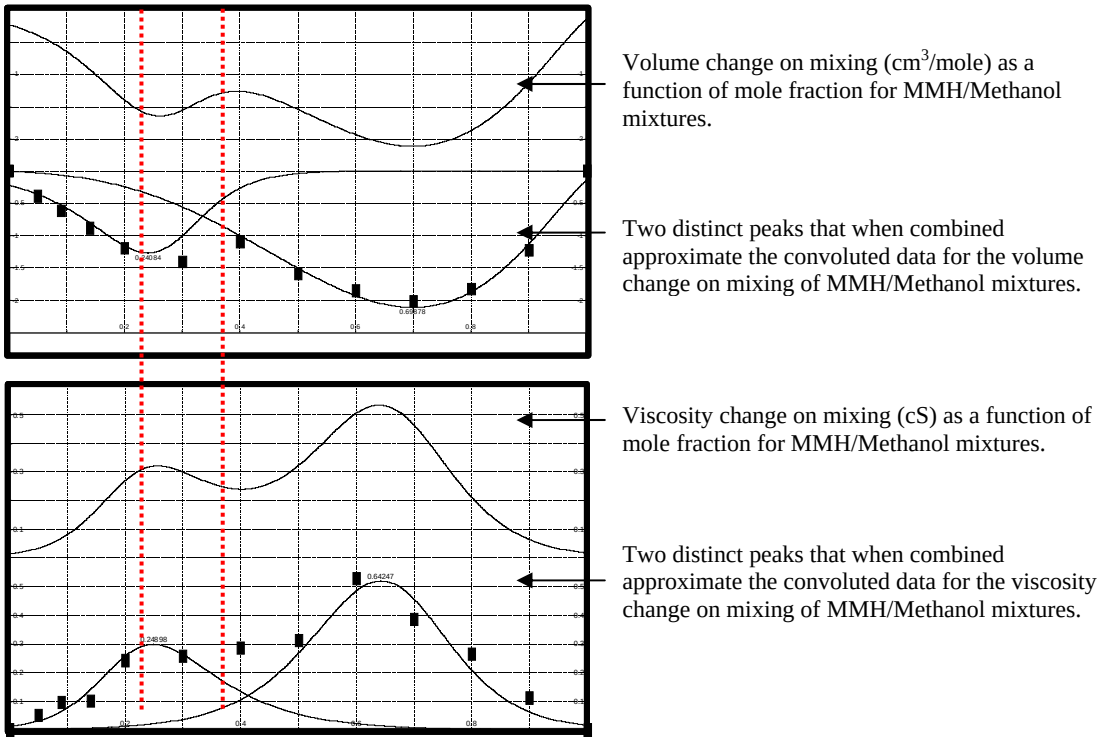

Figure 22: Molar Volume (upper) and Viscosity (lower) Changes on Mixing for MMH/Methanol Mixtures.

The difference in CDT across a given temperature range greatly affects the combustion performance of the fuels. A bipropellant with fast kinetics that only gets faster as temperature increases is of no concern. However, fuels with slow initial CDTs and large CDT variations with temperature, such as UDMH, should be of concern due to the unpredictable nature of the ignition delay during pulsed operations. From the results shown in Table 7, replacement fuels should exhibit small deviations in CDT as reactive temperature rises to reduce the possibility of uncontrolled reactions. Thus, the newly advanced modification to the Laser Diagnostic System can potentially be used to mitigate the risks associated with new fuel development and preliminary testing. Additional issues concerning the above are discussed by Dasarathy et al. (2005).

Table 4: Effect of Temperature on the CDT of Hydrazine

Temperature (K)	CDT (μs)	Standard Deviation (μs)
295	622	145
322	351	39.2
346	67.1	8.70
368	45.4	24.1

Table 5: Effect of Temperature on the CDT of UDMH

Temperature (K)	CDT (μs)	Standard Deviation (μs)
299	1073	128
311	1688	271
322	2584	162
333	2863	152

Table 6: Effect of Temperature on the CDT of MMH

Temperature (K)	CDT (μs)	Standard Deviation (μs)
300	546	55.6
315	346	46.2
328	301	53.2
344	255	62.8

Table 7: Relative Change in initial CDT Verses Temperature

Fuel	Temperature (K)	Initial Temperature CDT (μs)	Average CDT/ T (μs/K)
MMH	44.44	546	6.56
Hydrazine	72.22	622	7.99
UDMH	34.44	1073	51.97

As part of this project Chemical Delay Times of the fuels under development by AMRDEC were to be explored and compared to the benchmark replacement fuel MMH. Though various fuels and fuel mixture are being developed by AMRDEC only six were studied, as the fuel candidates have changed over the course of this research. These fuels experienced various responses to successive increases in fuel-lead temperature. These fuels listed in Table 8 were studied against RFNA and analyzed in the same manner as the hypergolic fuels examined in this report, however, due to sensitive nature, their results can not be reported here but are discussed in a separate technical report (Dasarathy and Smith 2006).

Table 8: Candidate Replacement Fuels Developed by AMRDEC

Fuel Abbreviation	Fuel Name
DMP	N,N'-Dimethylpiperazine
PMDETA	N,N,N',N',N''-Pentamethyldiethylenetriamine
TMEDA	N,N,N',N'-Tetramethylethylenediamine
DCPBD	1,4-Dicyclopropylbuta-1,3-diyne
DBN	Diazobicyclononane
DMAZ	2-azido-N,N-Dimethylethanamine

3.1.7 Modeling Temperature Effects

The Arrhenius Equation was used as the basis for modeling the temperature effect on the CDT of hypergolic bipropellants (Equation 1). By equating CDT to the rate constant (r) in Equation 1, we are able to determine activation energy, E_a, as well as a reaction constant, A, in Equation 2.

$$k = A \cdot e^{\left(\frac{-E_a}{R \cdot T}\right)} \quad (1)$$

$$CDT = A \cdot e^{\left(\frac{-E_a}{R \cdot T}\right)} \quad (2)$$

Using nonlinear regression, values for the reaction constant, A, and activation energy, E_a, were found for MMH and Hydrazine and are shown in Table 9. Activation energies for MMH and Anhydrous Hydrazine are on the same order of magnitude, ranging from -16.3 kJ to -40.7 kJ, while the reaction constant, A, ranges from 0.779 to 12.4 μs. Figures 23 and 24 show the results obtained using Equation 2 and the values from Table 9 for these fuel/oxidizer combinations. After examining the accuracy of the model, it is clear that Equation 2 captures the effect of temperature on CDT for MMH and Hydrazine. While the model proposed by Equation 2 does incorporate the change of temperature on the system, it does not account for the ratio of fuel to oxidizer, which has been proven to affect the chemical delay time of hypergolic bipropellant combustion (Farmer 1997). Nonlinear regression values for fuels under development by AMRDEC were also obtained using this manner and are reported by Dasarathy and Smith (2006).

Table 9: Predicted Model Based on Arrhenius Equation

Fuel	E_a (J/mol)	A (μs)
MMH	-1.63E+04	0.77941
Hydrazine	-4.0693E+4	1.23753E-4

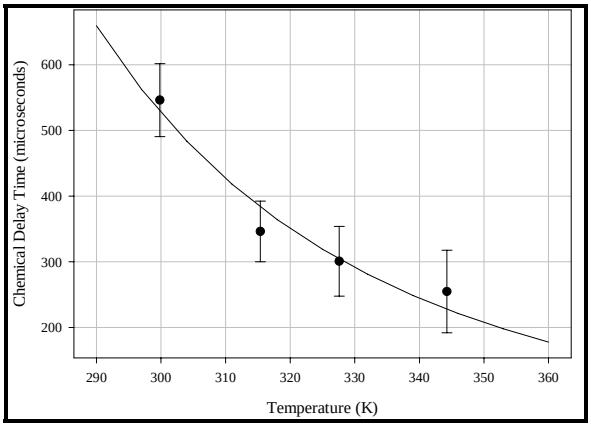

Figure 23: Predicted Values of CDT for MMH Based on the Arrhenius Equation

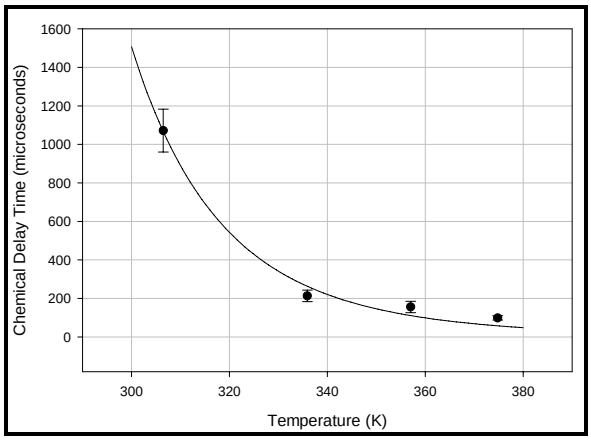

Figure 24: Predicted Values of CDT for Hydrazine Based on the Arrhenius Equation

Having established the ability to partially model the temperature effect on CDT for a given fuel at a single fuel-to-oxidizer ratio, the next step was to modify the model to predict the effect of changes in the fuel-to-oxidizer (F/O) ratio. This study was performed using hydrazine and RFNA, one of the most well studied hypergolic bipropellants. The temperature study was performed for three different F/O ratios: 2, 3, and 4 drops of fuel to 1 drop of oxidizer. For illustrative purposes, drop ratios are shown in Figure 25; however, calculations were carried out using molar ratios. As can be seen from Figure 25, increasing the F/O ratio for hydrazine increases the CDT. The increase in

temperature had a similar effect on all three F/O ratios, decreasing CDT with each incremental increase in temperature.

Since it is clear that F/O ratio plays an important role in the CDT of a given fuel, the next step was to modify the kinetic model previously used to incorporate this parameter. The significant impact of F/O ratio led to two separate equations, both of which can model the data. Equations 3 and 4 are both similar in nature, but since this paper refers to the ratio of fuel to oxidizer and doing so results in a dimensionless quantity, Equation 4 is preferred from a modeling perspective.

$$CDT = A \cdot \exp\left(\frac{-E_a}{R \cdot T}\right) \cdot F^m \cdot O^n \qquad (3)$$

$$CDT = A \cdot \exp\left(\frac{-E_a}{R \cdot T}\right) \cdot \left(\frac{F}{O}\right)^m \qquad (4)$$

Approximate values for the reaction constant, A, and activation energy, E_a, were found using the previous model and were used as initial guesses to determine values for A, E_a, and m in the kinetic model. The F/O ratio was entered as a mole ratio, determined by drop sizes and densities for both the fuel and oxidizer. By carrying out a multivariable optimization of Equation 4 using the appropriate CDT data shown in Figure 25, numerical values for the constants, A, E_a, and m were found and listed in Table 10. By further assuming that the constant, m, represents the overall reaction, further modification was required since an order of 0.66 was numerically determined. By setting m to the nearest half integer, 0.5, it is possible to finalize values for A and E_a, resulting in the values in Table 11. In either case, the kinetic model correlated the data as a function of both temperature and F/O ratio.

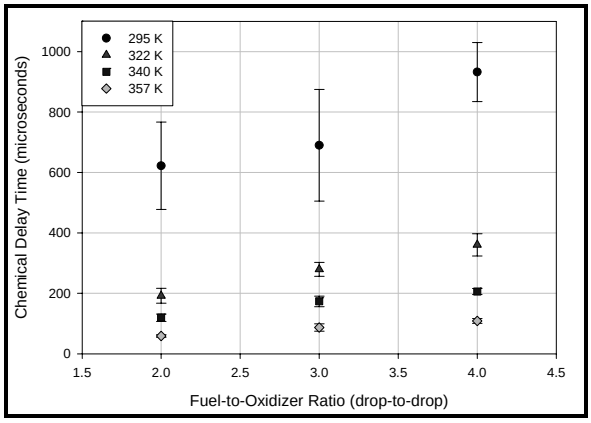

Figure 25: F/O Ratio and Temperature Effect on the CDT of Hydrazine

Table 10: Predictive Model Developed Through Multivariable Optimization

Equation Constant	Value	Units
A	1.37E-03	μs
E_a	-2.89E+04	$\frac{J}{mol}$
M	0.66	

Table 11: Predictive Model Using Fixed One-Half Reaction Order

Equation Constant	Value	Units
A	1.90E-03	μs
E_a	-2.90E+04	$\frac{J}{mol}$
M	0.5	

Figures 26-28 show the predicted values across the experimental temperature range, using the constants from Table 11, relative to the experimental CDT data obtained in this study. The model predicts the data with an average error of 10.9%. Thus, a kinetic model based on the measured chemical delay time appears to correlate to initial rate data for this hypergolic bipropellant, since the CDT is measured from the initial release of reactive gas to the initial appearance of the flame.

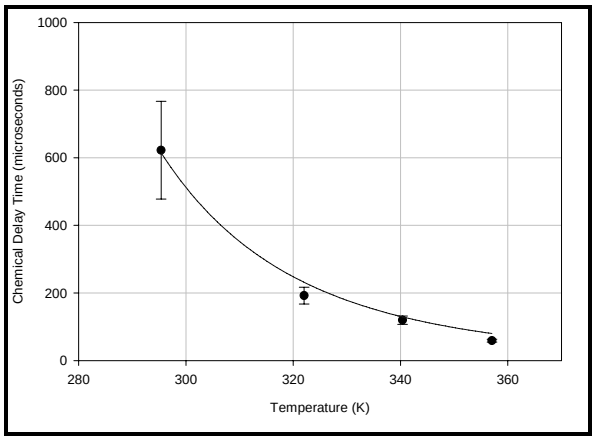

Figure 26: Predictive Model and Experimental Data for Hydrazine/RFNA Ratio of 2

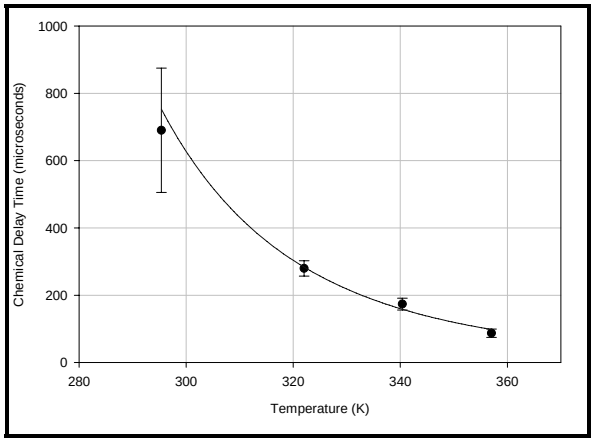

Figure 27: Predictive Model and Experimental Data for Hydrazine/RFNA Ratio of 3

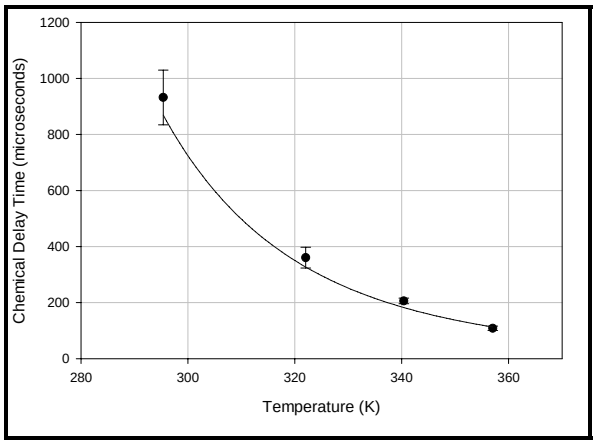

Figure 28: Predictive Model and Experimental Data for Hydrazine/RFNA Ratio of 4

3.1.8 Proposed Reaction Mechanism

The Ignition Delay Time (IDT) is a combination of three separate and distinct periods in the combustion of a hypergolic bipropellant. The phases consist of the addition of the oxidizer to the fuel droplet (points A-B), mixing and reaction within the liquid phase (points B-C) and gas evolution and combustion (points C-D), respectively in Figure 10. Thus, the classic IDT is the time from points A-D while the CDT is from points C-D. In further discussions, the time between points B and C will be referred to as the Liquid Reaction Time (LRT). It was previously assumed that the combination of oxidizer and fuel resulted in a mixture that generates enough heat to combust. For Hydrazine, this mixture occurs in the liquid phase, since Hydrazine gas does not react with nitric acid in the vapor phase (Schmidt 2001). Another proposed mechanism for combustion involves the creation of a reactive intermediary by way of an exothermic reaction between contacting liquids of Hydrazine and RFNA. The intermediary is heated by the reaction beyond its auto-decomposition temperature at which point it decomposes into reactive vapors that spontaneously ignite.

This latter mechanism is supported by previous studies into the effect of varying the carbon to nitrogen (C/N) ratio of the fuel being tested (Mays 1998). If one assumes that vaporization of the individual species is responsible for combustion, then the Chemical Delay Times should simply be the mole fraction additive of the pure components CDTs. That is, the CDT for any mixture of Hydrazine and UDMH should fall on a line stretching between the CDT for pure Hydrazine and pure UDMH. However, as can be seen from Figure 29 this does not explain the experimental phenomena. For a particular F/O ratio, a mixture of ~70:30 mole percent of Hydrazine and UDMH (Aerozine 50/50) resulted in a CDT of 300 μs, which is significantly lower than a 70:30 mole percent mixture of pure Hydrazine and UDMH that should be 1025μs if they are mole fraction additive. This mixture effect gives Aerozine 50/50 a CDT that rivals MMH/RFNA. Thus, a reaction between pure component vapors can not possibly explain the above results. Formation of reactive intermediates in the liquid phase is most probably responsible for the reduced CDTs when mixed fuels are involved. This is a topic for further research.

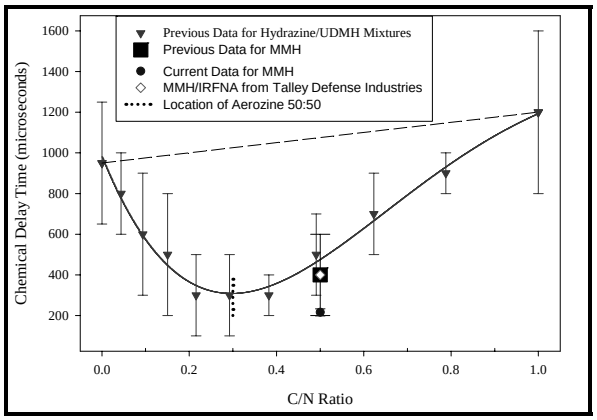

Figure 29: Effect of Mixing on the CDT of Hydrazine/UDMH

A more probable reaction mechanism for AH is the formation of a reactive intermediate that spontaneously decomposes at a higher temperature. One possible intermediate is ammonium nitrate, which is created by the mechanism of oxidative decomposition described by A.V. Anan'ev and V. P. Shilov (2004). The initiation step is described by the protonation of Hydrazine forming hydrazinium ions ($N_2H_5^+$). This ion reacts with other ionic species in the reacting propellant mixture leading to a series of reactive intermediates that eventually terminates at the formation of ammonium nitrate. As the temperature of the reacting liquid propellant increases it eventually exceeds the decomposition temperature of ammonium nitrate (210^{o}C), point C, followed by combustion, point D in Figure 10, respectively (Sax 1987).

When analyzing Figure 25 it was noticed that the standard deviation of the CDT decreased with increasing temperature for all three F/O ratios. Experimental error was the first considered to explain this phenomenon; however, the order of experiments was determined by the F/O ratio rather than temperature thereby eliminating this possibility. In order to justify the decrease in error a physical explanation was therefore necessary. As the CDTs had previously been measured, the same data were used to determine the liquid reaction times (LRTs) at the same F/O ratios and temperatures. The resulting LRTs are shown in Figure 30. At 295 K, the average reaction time for all three F/O ratios was 89.9 ms. This time reduces significantly to 17.5, 14.4, and 10.1 ms as temperature is increased to 355 K. One explanation for this trend is that the vaporization rate is increased significantly with the increase in temperature; however, the conclusions reached above better support an increase in the production rate of the reactive intermediate. While the reaction time does decrease with increasing temperature, at a given temperature the reaction time does not statistically differ for F/O ratios of 2, 3, and 4. By adding significant energy to the system, the reactive intermediates are formed at a greater rate which results in reduction of LRT shown in Figure 30. The shorter LRT reduced the variability in the amount of ammonium nitrate being produced, thereby reducing the standard deviation as seen in Figure 25. The rapid rate of production of the intermediates at higher temperatures also leads to a greater rate of release of combustible decomposition products from the intermediates, resulting in reduced Chemical Delay Times as shown in Figure 25. In addition, as the initial temperature of the fuel is increased, the difference between the reaction temperature and ammonium nitrate decomposition temperature narrows following the recently proposed mechanism of A.V. Anan'ev and V. P. Shilov (2004).

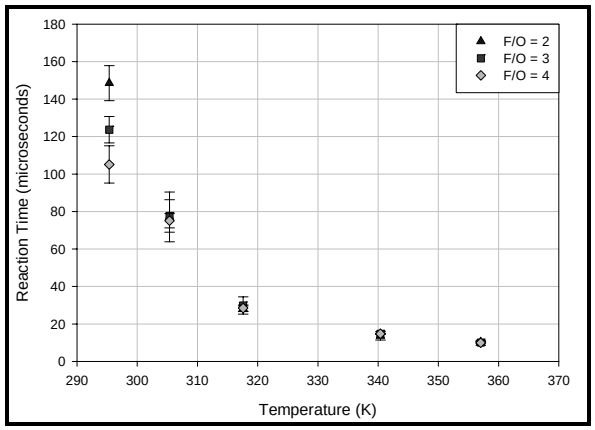

Figure 30: Temperature Effect on Reaction Time for Hydrazine/RFNA

3.1.9 Modeling Liquid Reaction Time

The process used to develop a predictive model for the Liquid Reaction Time data was similar to that used to model Chemical Delay Times. Equation 5 was optimized from data used to obtain Figure 30. Upon completion of the multivariable optimization, values for the reaction constant, A, activation energy, E_a, and m, were found and are shown in Table 12.

$$LRT = A \cdot \exp\left(\frac{-E_a}{R \cdot T}\right) \cdot \left(\frac{F}{O}\right)^m \qquad (5)$$

By again assuming that the constant, m, represented the overall reaction order, modification was again necessary since an order of -0.352 was numerically determined. The value for the overall reaction order was set to

the nearest half integer, -0.5, in order to establish values for A and E_a. This resulted in the values in Table 13. The negative order can be considered scientifically valid since it essentially means an O/F ratio must be used in place of the F/O ratio. The results of the model for various O/F ratios are shown in Figures 31-33.

Table 12: Predictive Model Developed Through Multivariable Optimization

Equation Constant	Value	Units
A	4.52E-06	μs
E_a	-4.39E+04	$\frac{J}{mol}$
M	-0.352	

Table 13: Predictive Model Using Fixed Negative One-Half Reaction Order

Equation Constant	Value	Units
A	3.80E-06	μs
E_a	-4.51E+04	$\frac{J}{mol}$
M	-0.5	

Equation 5 with the appropriate values from Table 13 predicts experimental data with an average error of approximately 21%. This error is most likely related to variations in transport effects associated with reactive liquid mixing. However, the relative fit does indicate that the experimental data experiences and exponential decrease in Liquid Reaction Time similar to the predictive model, relative to successive increases in temperature. It is interesting to note that the Arrhenius constant decreases by three orders of magnitude relative to the CDTs in the gas phase since the intermediate reaction occurs in the liquid phase. The kinetic nature of both the LRT and CDT supports the assumption that Anhydrous Hydrazine and RFNA react in the liquid phase to form an intermediate species that then decomposes and combusts.

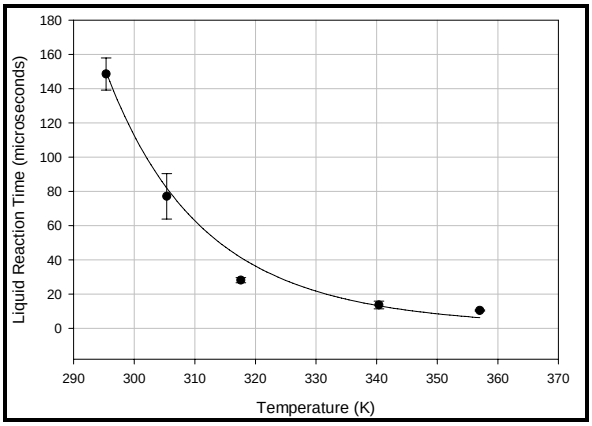

Figure 31: Predictive Model and Experimental Data for the Hydrazine/RFNA Ratio of 2

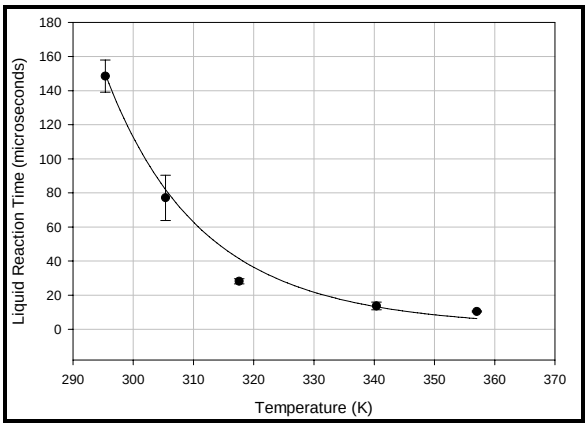

Figure 32: Predictive Model and Experimental Data for the Hydrazine/RFNA Ratio of 3

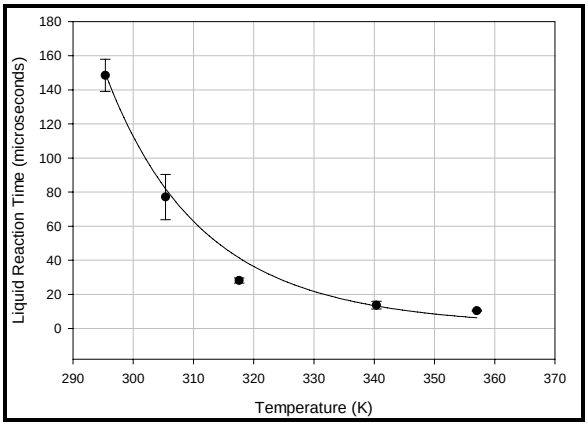

Figure 33: Predictive Model and Experimental Data for the Hydrazine/RFNA Ratio of 4

3.1.10 Liquid Reaction Temperature

The procedure used to determine liquid reaction temperature was similar to that of the previous study of the temperature effect on chemical delay time. Since the speed of the reaction was not being considered, the laser/detector system used to determine Chemical Delay Times was not incorporated into this study. Before the fuel lead was placed on the combustion plate, the thermocouple was positioned such that the loop, described in Section 2.1.4, was flat against the combustion plate. With the thermocouple in place, approximately three drops of fuel lead was placed on the combustion plate to sufficiently submerge the thermocouple loop in the liquid. After this had been accomplished, the automated syringe delivered a single drop of oxidizer while the data acquisition system recorded the temperature of the liquid during the reaction and combustion phases. The data obtained from the DaqView software was a temperature versus time profile.

The purpose of capturing the temperature profile of the liquid phase reaction between Anhydrous Hydrazine and Red Fuming Nitric Acid was to attempt to confirm the formation of a reactive intermediate. Since it has been proposed that the reaction between AH and RFNA produces a vapor that is responsible for combustion, it was hypothesized that the vapor creation was due to the auto-decomposition of the reactive intermediate. By determining at what temperature the reactive intermediate was decomposing, it was also hypothesized that this would confirm that ammonium nitrate was a possible reactive intermediate.

Figure 34 is an example of a temperature profile where the thermocouple had reading points outside the liquid phase and in the flame region. Since the thermocouple has a range of operability, once the flame reaches a temperature above 1260 °C the data acquisition is unable to record temperatures. When the temperature returns below the upper limit, temperatures are again recorded. Since the heating and cooling times of the thermocouple are not the same, it is not possible to extrapolate for the unrecorded sections in order to determine the time at which maximum flame temperature is reached.

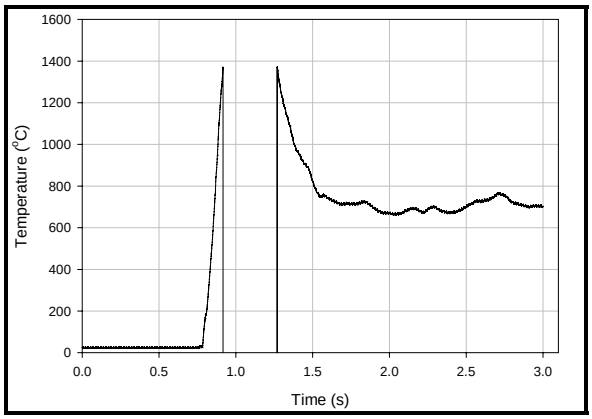

Figure 34: Temperature vs. Time Profile with Thermocouple in Flame Region

Table 14 contains the average maximum temperatures reached during two different stages of experimentation. At first, temperature measurements were taken with the fuel lead at room temperature. After obtaining temperatures ranging from approximately 80 °C to 170 °C, it was postulated that starting the fuel at slightly above room temperature would reduce variability. The ceramic heating stage allowed for the fuel to be preheated to above room temperature to compensate for any heat sinks that might be present within the system as well. After conducting a series of experiments during which the fuel lead was preheated, data from both sets were compared. While the average maximum temperature was not significantly different, the standard deviation of the preheated fuel experiments had decreased. The two standard deviations were statistically compared and were found to be different at a 95% confidence. From this, it can be inferred that conducting the experiments in a preheated environment increases the precision of the results.

Table 14: Average Maximum Temperatures of Hydrazine/RFNA Reaction

	Average Maximum Temperature	Standard Deviation
Room Temperature	129.26	28.81
Preheated Fuel	139.05	16.46

Figure 35 shows the average maximum temperatures reached for each trial and their corresponding standard deviations. Experiments 1 and 3 were conducted at room temperature while 2, 4, and 5 received a preheat temperature. It can be seen from the decrease in error bars that precision increased in Experiments 2, 4, and 5. Standard deviations for Experiments 1 and 3 were compared and found not to be statistically different; the same was determined when comparing combinations of Experiments 2, 4, and 5.

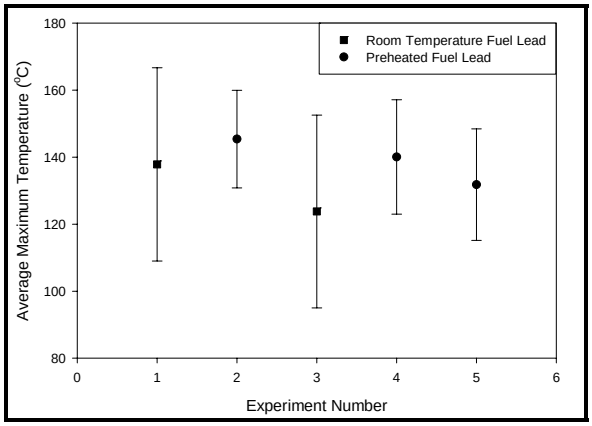

Figure 35: Effect of Preheat Temperature on Standard Deviations

Figures 36 and 37 illustrate experiments during which the thermocouple remained submerged in the liquid phase. In Figure 36, the temperature of the system peaked at 138 °C, while the temperature in Figure 37 peaked at 156 °C. The average peak temperature for all experiments was found to be 135 ± 23 °C. This average consists of two different stages of experimentation discussed previously. The average temperature of 135 °C was found to be lower than the expected auto-decomposition temperature of ammonium nitrate (210 °C) responsible for combustion. The auto-decomposition temperature for ammonium nitrate is a temperature that is a result of a completely adiabatic system. The non-adiabatic nature of the current apparatus would therefore result in a lower temperature reading. Heat sinks present within the system include the thermocouple itself, the ceramic combustion plate, and the attached components. Radiation and convection of heat to the surroundings would also reduce the temperature of the liquid phase read by the thermocouple. Because of the inability to control these boundary conditions, it was reasonable that the temperature of the liquid phase did not reach the predicted adiabatic auto-decomposition temperature of ammonium nitrate.

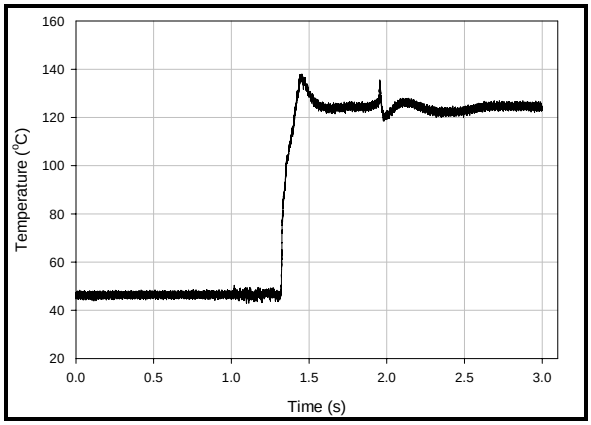

36: Liquid Phase Temperature Profile for Pre-heated Hydrazine/RFNA Reaction

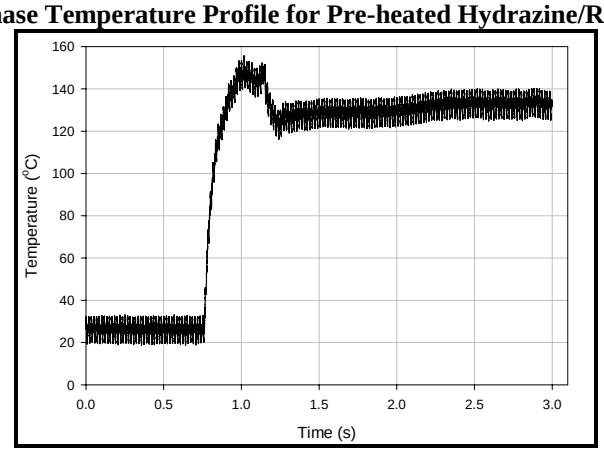

Figure 37: Liquid Phase Temperature Profile for Room Temperature Hydrazine/RFNA Reaction

4.0 CONCLUSIONS AND RECOMMENDATIONS

A drop test technique was refined that provides additional information over past techniques. The only measurement that can be quantitatively compared between various researchers is the chemical delay time. The chemical delay time varies substantially due to mixed fuel compositions and oxidizer to fuel ratios and is an important tool to understand the chemistry occurring during ignition and combustion of hypergolic bipropellants. Ultimately, this will lead to the development of safer more effective hypergolic fuels.

Results showed that oxygen from air contributes significantly (23%) to the MMH/RFNA; however, hydrazine and UDMH reacted with RFNA showed only a slight influence that was within the experimental error. The presence of a vortex ring was proposed that in essence creates a micro reactor within the oxidizer pool at the free surface between the reactants**.** The presence of a vortex ring may ultimately limit the molar flux to the reaction zone limiting the kinetics by decreasing combustion efficiency.

The presence of carbon influences the Chemical Delay Time, clearly showing that carbon is important to the reaction mechanism. It is also obvious that too much carbon or no carbon at all slows the reaction. Therefore it was

beneficial to further detail the importance of the carbon to nitrogen ratios in hydrazine mixtures. This result suggests that adding an asymmetric polar compound, such as MMH, could reduce the CDT for other hydrazines or azides.

The addition of Methanol to hydrazines as an internal source of oxygen altered the CDT for MMH but not UDMH and Hydrazine. For certain MMH/Methanol mixtures the CDT decreased from that of pure MMH, therefore, for MMH/Methanol mixtures < 23 mole % Methanol the mixtures are chemically faster than pure MMH and for MMH/Methanol mixtures > 23 mole % the CDT increases from that of pure MMH. Different combustion mechanisms as a function of Methanol concentration were observed and included both stable hypergolic combustion below 25 mole % Methanol and unstable or explosion above 40 mole % Methanol. MMH/Methanol mixtures also produce a volume change on mixing, heat of mixing and viscosity change on mixing. All mixing data showed degrees of convolution. These data required two peaks to deconvolute the phenomena. In general the maxima in the first peak and minima between the first and second peak approximated the boundaries of stable and meta-stable combustion, respectively.

The increase in initial fuel temperature has varied effects on the Chemical Delay Time depending on the fuel being tested. It was shown that the majority of fuels respond with a decrease in CDT for an incremental increase in temperature. With the ability to collect CDT data at various temperatures, it was shown that the hypergolic reaction between oxidizer and fuel as measured by the CDT appears to be a measure of kinetic behavior. The results from the preliminary kinetic modeling of the relationship between CDT and temperature show an Arrhenius-like behavior for many of the pure components tested to date. Additional studies are necessary to generalize this conclusion. The model was extended to include the F/O ratio for Hydrazine and RFNA with the results correlated to an average error of 10.9 percent and thereby appears to predict the kinetic behavior of these two reactants.

A second conclusion concerns the initial CDT and variations in the CDT with respect to temperature. A bipropellant with fast kinetics that only gets faster is of no concern. Fuels with slower initial CDTs and larger CDT variations with temperature, such as UDMH, should be of concern due to the unpredictable nature of the ignition delay during pulsed operations. Replacement fuels should exhibit small deviations in CDT as reactive temperatures rise to reduce the possibility of uncontrolled reactions.

As a result of the kinetic analysis a reaction mechanism controlled by reactive intermediates formed in the liquid phase, which spontaneously decompose at high temperatures, was advanced. One possible intermediate is ammonium nitrate, which may be created by the mechanism of oxidative decomposition described by A.V. Anan'ev and V. P. Shilov (2004). This ion reacts with other ionic species in the reacting propellant mixture leading to a series of reactive intermediates that eventually form ammonium nitrate. As the temperature of the reacting propellant increases it eventually exceeds the decomposition temperature of ammonium nitrate (210^{o}C) at which point spontaneous decomposition followed by ignition occurs.

Examination of the liquid reaction time (LRT) verses O/F ratio also fit a kinetic equation for the differential time decrease in the LRT as a function of temperature. It is interesting to note that the Arrhenius constant decreases by three orders of magnitude relative to the CDTs in the gas phase since the intermediate reaction occurs in the liquid phase. The kinetic nature of both the LRT and CDT supports the assumption that Anhydrous Hydrazine and RFNA react in the liquid phase to form an intermediate species that then decomposes and combusts.

An attempt was made to measure the liquid temperature during this reactive phase. The liquid did heat rapidly; however, it did not reach the adiabatic auto-decomposition temperature for ammonium nitrate. The non-adiabatic nature of the current apparatus would therefore result in a lower temperature reading. Heat sinks present within the system include the thermocouple itself, the ceramic combustion plate, and the attached components. Radiation and convection of heat to the surroundings would also reduce the temperature of the liquid phase read by the thermocouple. Because of the inability to control these boundary conditions, it was reasonable that the temperature of the liquid phase did not reach the predicted adiabatic auto-decomposition temperature of ammonium nitrate.

The kinetic modeling of the CDTs in the vapor phase was applied to research fuels under development by AMRDEC. However, due to their sensitive nature they were reported elsewhere (Dasarathy and Smith 2006).

Spectroscopic techniques could not be directly measured due to the extreme rapid nature of the CDT region, large flame emission once the reaction began, and long detector exposure times relative to the reactive regimes. However, techniques have been advanced to probe the bulk kinetics of both the vapor and liquid phases of hypergolic bipropellants. These techniques are of interest to various companies and other components of the Department of Defense, as evidence by the following section.

5.0 TECHNOLOGY TRANSFER

Our research group made micro-combustion measurements on advanced hypergolic bipropellants, supporting the following companies SBIR awards with Ogden Engineering now receiving a phase II study of a hypergolic fuel

important to the Air Force. In addition, AMRDEC has recently approached our research group to examine various fuel mixtures based on preliminary data reported by Dasarathy and Smith (2006) and the results obtained by Dasarathy et al. (2005). We expect to see more interest associated with kinetic measurements as this technique receives greater acceptance.

- 3 D RESEARCH CORP.
  7057 Old Madison Pike, Suite 200 P.O. Box 11723
  Huntsville, AL 35806
  MDA 04-099 Advanced Gel Propellants for Exo Atmospheric Kill Vehicle for Ground Based Midcourse Defense (GMD).

- OGDEN ENGINEERING & ASSOC., LLC
  8180 N. Placita Sur Oeste, Tucson, AZ 85741
  MDA 04-170 Hypergolic Green Fuel Formulation

6.0 ACKNOLEDGEMENTS

This material is based upon work supported by, or in part by, the U. S. Army Research Laboratory and the U. S. Army Research Office under grant number DAAD190210356.

7.0 REFERENCES

Anderson, B. B., "Hypergolic Testing and Hazards Evaluation of Amine/Azide Compounds," Technical Laboratory Report Number 683, Final Report prepared for TRW Space Electronics Group, Redondo Beach, CA, 1999a. (Limited Distribution).

Anderson, B. B., "Tertiary Amine Azide Hypergolicity and Hazards Evaluation," 1999 JANNAF SEPS/PDCS Meeting, San Diego, CA, April 1999 (Limited Distribution).

Balzhiser, R. E., Samuels, M. R., Eliassen, J. D., Chemical Engineering Thermodynamics: The Study of Energy, Entropy, and Equilibrium., Prentice-Hall, New Jersey, (1972).

Broatch, J. D., "An Apparatus for the Measurement of Ignition Delays of Self-Igniting Fuels," *Fuels*, Vol. 29, 1950, pp. 106-109.

Dasarathy, R. and Smith, Jr., J.E. "A CDT Study of Candidate MMH Replacement Fuels Under Development by AMRDEC," ARO Technical Report, 2006.

Dasarathy, R., Hampton C., and Smith, Jr., J.E. "The Relationship Between the Chemical Delay Time and Temperature for Hypergolic Bipropellants," 53rd JANNAF Propulsion Meeting/2nd Liquid Propulsion Subcommittee, Monterey, CA, December 2005

Dean, J. A., Handbook of Organic Chemistry., McGraw-Hill; New York, (1987).

Dooley, B. S., Warncke, A. E., Grarib, M. and Tryggvason, G., *Vortex Ring Generation Due to the Coalescence of a Water Drop at a Free Surface*, Experiments in Fluids, 22, **5**, 369-374, (1997).

Gunn, S. V., "The Effects of Several Variables upon the Ignition Lag of Hypergolic Fuels Oxidized by Nitric Acid," *ARS Journal*, Vol. 22, No. 1, pp. 33-38.

Hampton, C. S., Kelly, A.R., and Smith, Jr., J. E., "The Effects of Oxygenating Hydrazines on the Chemical Delay Time and Relative Toxicity," 52nd JANNAF Propulsion Meeting/1st Liquid Propulsion Subcommittee, Las Vegas, NV, May 2004.

Hampton, C. S., Ramesh, K. K., Berry, J. B., Smith, Jr., J. E., "Atmospheric Effects on the Chemical Delay Time for Hypergolic Bipropellants," AIAA Paper 2004-1381, AIAA 42nd Aerospace Sciences Meeting and Exhibit, Reno, NV, January 2004.

Kilpatrick, M., and Baker, L., *Fifth Symposium on Combustion*, New York-London, 1955, pp. 170-196.

Ladanyi, D. J., and Miller, R. O., "Two Methods for Measuring Ignition Delay of Self-Igniting Rocket Propellant Combinations," *Jet Propulsion*, Vol. 26, No. 3, pp. 157-63.

Mays, L. O., "Analysis of chemical Delay Time in Hypergolic Fuel and Fuel Mixtures," Masters Thesis, Department of Chemical and Materials Engineering, University of Alabama in Huntsville, September, 1998.

Paushkin, Y. M., *The Chemical Composition and Properties of Fuels for Jet Propulsion*, Pergamon Press, New York, 1962, p. 327.

Pino, M. A., "A Versatile Ignition Delay Tester for Self-Igniting Rocket Propellants", *Jet Propulsion*, Vol. 25, No. 9, pp. 463-466.

Purvis, R. and Smith, F.T., "Large Droplet Impact on Water Layers," AIAA Paper 2004-414, AIAA 42nd Aerospace Science Meeting and Exhibit, Reno, NV, January 2004.

Qian, J. and Law, C.K. "Regimes of coalescence and separation in droplet collision." *Journal of Fluid Mechanics*, Vol. 331, pp. 59-80, 1997.

Saad, M. A., and Goldwasser, S. R., "Role of Pressure in Spontaneous Ignition," *AIAA Journal*, Vol. 7, No. 8, pp. 1574-1581.

Schmidt, Eckart W., Hydrazine and its Derivatives., Vol. 1 and Vol. 2., Wiley-Interscience; New York, (2001).

Spengler, G. and Bauer, J., "Ignition Delay of Hypergolic Rocket Propellants," *Technical Translation 16 - U.S. Army*, June 1966.

8.0 LIST OF ALL PUBLICATIONS AND TECHNICAL REPORTS

Papers published in peer-reviewed journals

Farmer, M. J., Mays, L. O., Hampton, C. S., and Smith, Jr., J. E., "Reaction Rates for Hypergolic Propellants Using Chemical Delay Times," *Journal of Propulsion and Power,* Vol. 20, No. 2, 2004, pp. 372 – 376.

Papers published in non-peer-reviewed journals or in conference proceedings

Hampton, C. S., Ramesh, K. K., and Smith, Jr., J. E., "Importance of Chemical Delay Time in Understanding Hypergolic Behaviors," AIAA Paper 2003-1359, AIAA 41st Aerospace Science Meeting and Exhibit, Reno, NV, January 2003.

Hampton, C. S., Ramesh, K. K., Berry, J. B., Smith, Jr., J. E., "Atmospheric Effects on the Chemical Delay Time for Hypergolic Bipropellants," AIAA Paper 2004-1381, AIAA 42nd Aerospace Sciences Meeting and Exhibit, Reno, NV, January 2004.

Hampton, C. S., and Smith, Jr., J. E., "Mixture Effects on Hypergolic Bipropellant Combustion," 52nd JANNAF Propulsion Meeting/1st Liquid Propulsion Subcommittee, Las Vegas, NV, May 2004.

Hampton, C. S., and Smith, Jr., J. E., "The Effects of Oxygenating Hydrazines on the Chemical Delay Time and Relative Toxicity," 52nd JANNAF Propulsion Meeting/1st Liquid Propulsion Subcommittee, Las Vegas, NV, May 2004.

Hampton, C. S., and Smith, Jr., J. E., "The Importance of Carbon, Nitrogen and Oxygen Atomic Ratios on the Combustion of Hypergolic Bipropellants," AIAA Paper 2005-740, AIAA 43rd Aerospace Sciences Meeting and Exhibit, Reno, NV, January 2005.

Dasarathy, R., Hampton C., and Smith, Jr., J.E. "The Relationship Between the Chemical Delay Time and Temperature for Hypergolic Bipropellants," 53rd JANNAF Propulsion Meeting/2nd Liquid Propulsion Subcommittee, Monterey, CA, December 2005

Papers presented at meetings, but not published in conference proceedings

Smith, Jr., J. E., "Time Resolved Measurements and Reactive Pathways for Hypergolic Bipropellant Combustion," ARO-AFOSR Contractors' Meeting in Chemical Propulsion, Williamsburg, VA, June 23 – 25, 2003.

Smith, Jr., J. E., "Time Resolved Measurements and Reactive Pathways for Hypergolic Bipropellant Combustion," ARO-AFOSR Contractors' Meeting in Chemical Propulsion, Tucson, AZ, June 7 – 9, 2004.

Technical reports submitted to ARO

Dasarathy, R. and Smith, Jr., J.E. "A CDT Study of Candidate MMH Replacement Fuels Under Development by AMRDEC," ARO Technical Report, 2006.

9.0 LIST OF ALL PARTICIPATING SCIENTIFIC PERSONELL

Dr. James E. Smith Jr.
Krishna Ramesh – Master's Degree
Casey S. Hampton – Master's Degree pending
Raghava Dasarathy – Master's Degree pending

10.0 REPORT OF INVENTIONS BY TITLE ONLY

Oxygenation of Hypergolic Fuels for Increased Performance and Lower Toxicity (November 2004)